June 1991 • SERI/TP-214-4226

PROPERTY OF
U. S. GOVERNMENT

Research on Stable, High-Efficiency, Large-Area, Amorphous-Silicon-Based Submodules

Final Subcontract Report
16 March 1989 - 15 October 1990

SOLAR ENERGY RESEARCH INSTITUTE
TECHNICAL LIBRARY
JUL 30 1991
GOLDEN, COLORADO 80401

A.E. Delahoy
T. Tonon
J. Macneil
Chronar Corporation
Princeton, New Jersey

olar Energy Research Institute
division of Midwest Research Institute
perated for the U.S. Department of Energy
nder contract No. DE-AC02-83CH10093

SERI/TP-214-4226 c.2

SERI/TP-214-4226 • UC Category: 271 • DE91002167

SERI/TP--214-4226

DE91 002167

Research on Stable, High-Efficiency, Large-Area, Amorphous-Silicon-Based Submodules

Final Subcontract Report
16 March 1989 - 15 October 1990

A.E. Delahoy
T. Tonon
J. Macneil
Chronar Corporation
Princeton, New Jersey

SERI technical monitor: W. Luft

Solar Energy Research Institute
1617 Cole Boulevard
Golden, Colorado 80401-3393
A Division of Midwest Research Institute
Operated for the U.S. Department of Energy
under Contract No. DE-AC02-83CH10093

Prepared under Subcontract No. ZB-7-06003-1

June 1991

MASTER

DISTRIBUTION OF THIS DOCUMENT IS UNLIMITED

This publication was reproduced from the best available camera-ready copy submitted by the subcontractor and received no editorial review at SERI.

NOTICE

This report was prepared as an account of work sponsored by an agency of the United States government. Neither the United States government nor any agency thereof, nor any of their employees, makes any warranty, express or implied, or assumes any legal liability or responsibility for the accuracy, completeness, or usefulness of any information, apparatus, product, or process disclosed, or represents that its use would not infringe privately owned rights. Reference herein to any specific commercial product, process, or service by trade name, trademark, manufacturer, or otherwise does not necessarily constitute or imply its endorsement, recommendation, or favoring by the United States government or any agency thereof. The views and opinions of authors expressed herein do not necessarily state or reflect those of the United States government or any agency thereof.

Printed in the United States of America
Available from:
National Technical Information Service
U.S. Department of Commerce
5285 Port Royal Road
Springfield, VA 22161

Price: Microfiche A01
Printed Copy A04

Codes are used for pricing all publications. The code is determined by the number of pages in the publication. Information pertaining to the pricing codes can be found in the current issue of the following publications which are generally available in most libraries: *Energy Research Abstracts (ERA)*; *Government Reports Announcements* and Index (*GRA* and I); *Scientific and Technical Abstract Reports (STAR)*; and publication NTIS-PR-360 available from NTIS at the above address.

PREFACE

This Final Technical Report covers research performed by Chronar Corporation under Subcontract No. ZB-7-06003-1 during the period of March 16, 1989 to October 15, 1990. This period represents phase III of a 3-phase, cost-shared research program. Emphasis is placed in this report on results obtained during the second half of phase III, since research performed during the first half has already been published in the relevant semi-annual subcontract report. Individuals who have contributed to the results described here include:

Mr. J. A. Cambridge
Mr. H. Chao
Dr. A. E. Delahoy, Principal Investigator, Subtasks B1/B2.
Dr. F. B. Ellis, Jr.
Mr. H. Field
Ms. M. Ghosh
Mr. C. Huang
Dr. F. J. Kampas
Mr. C. Kothandaraman
Ms. X. Li
Dr. R. Liu
Dr. T. Liu
Dr. J. Macneil, Program Manager
Mr. J. O'Donnell
Mr. R. Radeztsky
Mr. F. Ramos
Dr. H. Schade
Mr. W. Stroud
Mr. D. Talenti
Dr. T. Tonon, Principal Investigator, Subtask B3
Dr. H. A. Weakleim
Dr. J. Xi

TABLE OF CONTENTS

		Page
	Preface	i
	Table of Contents	ii
	List of Figures	v
	List of Tables	vii
	SUMMARY	iiiv
1.0	INTRODUCTION	1
2.0	SEMICONDUCTOR MATERIALS AND SMALL AREA CELLS	2
	2.1 Deposition of Amorphous Silicon	2
	2.1.1 Features of the D2-system	3
	2.2 I-layer Properties	3
	2.2.1 Long Diffusion Length of D1-system Material	3
	2.2.2 Opto-electronic Properties of D2 and B System Material	5
	2.2.3 Directions for Further I-layer Development	5
	2.2.3.1 Enhanced Optical Absorption	10
	2.3 P-layer Research	10
	2.3.1 Variation of P-layer Properties in Girection of Gas Flow	10
	2.3.2 Influence of Diborane Concentration on Cell Uniformity	11
	2.3.3 Use of Trimethylboron as a P-type Dopant Source	14
	2.4 High Efficiency Single Junction Cells	16
	2.4.1 Cells with TMB P-layers	16
	2.4.2 Cells with Diborane P-layers	16

2.4.3 Cells from the New D2-system 20
2.5 Tandem Junction Cells 20
2.6 Photostability 22
2.6.1 Effect of Silicon Carbide Transitional I-layer on Photostability 22
2.6.2 Post-deposition Modification of Cell Stability 24
2.6.3 Influence of Contact Materials on Photostability 24
3.0 NON-SEMICONDUCTOR MATERIALS 26
3.1 Front Contact Materials 26
3.1.1 Tin Oxide 26
3.1.2 Tin Oxide Overcoated with Zinc Oxide 26
3.2 Sputtered Back Contact Materials 28
3.2.1 Sputtering-induced Damage In p-i-n Devices 28
3.2.2 Back Contact Annealing Studies 29
3.2.3 Preparation and Properties of Sputtered Zinc Oxide Films 29
3.2.4 Zinc Oxide Based Back Reflectors 32
4.0 SUBMODULE RESEARCH 35
4.1 Approach to Submodule Fabrication 35
4.2 Power Losses in Submodules 35
4.2.1 Front TCO Sheet Resistance 35
4.2.2 Contact Resistance in Interconnection 36
4.2.3 Shunts 36
4.2.3.1 Shunt Quality 36

4.2.3.2 Types of Shunts 38

4.2.3.3 Shunting Power Loss 38

4.2.4 Patterning Losses 40

4.2.5 Nonuniform Deposition and Mismatching 40

4.3 Laser Patterning 41

4.3.1 2-step Fused Interconnecton 41

4.3.2 3-step Laser Scribing with Computerized Tracking 42

4.3.3 Laser/Etch Technique for Back Contacts 42

4.3.4 Annealing and Laser Performance 43

4.4 Best Module Performance 43

4.4.1 Single Junction 43

4.4.2 Tandem Junction 46

REFERENCES 47

LIST OF FIGURES

Figure		Page
1.	Block diagram of the D2 a-Si:H deposition system	4
2.	Thickness map for a-Si:H deposited on a 1 ft^2 substrate in the D2-system.	6
3.	Log - log plot of photoconductivity versus light intensity for a D2-system i-layer	7
4.	Log - log plot of photoconductivity versus light intensity for a B-system i-layer	8
5.	Dark conductivity versus 1/T (activation energy plot) for the B-system i-layer of Fig. 4.	9
6.	Spatial variation of the spectral response and overall photovoltaic parameters of p-i-n cells caused by the variation of their p-layer composition in the direction of gas flow	12
7.	Dark conductivity versus bandgap for a-$Si_{1-x}C_x$:H p-layers doped using either diborane or trimethylboron	15
8.	J-V curve for a 10.5% cell employing a TMB p-layer, ZnO/Ag reflector, but no transitional i-layer	17
9.	J-V curve for an 11.3% cell (area 1.05 cm^2) employing a diborane p-layer and ZnO/Ag reflector	18
10.	J-V curve obtained by SERI for a cell having the structure defined in Fig. 9	19
11.	J-V curve for a 9.3% tandem junction cell with TiO_x interstack recombination layer	21
12.	Percent change in fill factor (referred to initial fill factor) versus anneal temperature for cells with evaporated Al back contacts and sputtered Al (2% Si) back contacts when subjected to 20 minute periods of annealing at successively higher temperatures.	30

13. Transmission spectrum of 9.5 Ω/□ ZnO:Al (sputtered) compared with that of 10.5 Ω/□ SnO_2:F (APCVD) 31
14. Measured percent power of a 1 cm x 30 cm cell as a function of shunt resistance 37
15. Correlation between actual module percent power and that calculated from shunt quality, Q_s 39
16. I-V curve for a 1 ft^2 single junction module with ZnO/Al reflector (aperture area efficiency 7.55%) 44
17. Outdoor measurements on a 1.2m^2 Eureka module; power output 74.4 W, a world record for a monolithic thin film module. (Data acquired on April 6, 1990 at the SERI PV module testing and performance faciity) 45

LIST OF TABLES

		Page
I.	Performance of amorphous silicon cells and modules (single and tandem junction)	X
II.	Opto-electronic properties of D2 - system and B - system i-layers	5
III.	Variation of a-$Si_{1-x}C_x$:H p-layer properties as a function of position in the direction of gas flow; the gas mixture consists of silane, methane and diborane.	11
IV.	Distribution of cell efficiency across a 1 ft^2 substrate as a function of diborane concentration in p-layer gas mixture.	13
V.	Average efficiency of cells with and without a transitional i-layer (i_t) as a function of light soak time.	23
VI.	Percent change in single junction PV parameters upon light soaking.	23
VII.	Comparison of the photostability of thick, single junction cells deposited simultaneously on SnO_2 and SnO_2/ZnO.	25
VIII.	Comparison of the photostability of cells metallized with Al and ZnO/Al.	25
IX.	Average PV parameters for p-i-n cells on SnO_2 and SnO_2/ZnO as a function of back contact type and number of anneals.	27
X.	Dependence of sheet resistance upon time of annealing at 150°C for 800A ZnO:Al films annealed in air and argon.	32
XI.	Performance of cells metallized with various back reflectors and subjected to successive annealings.	33
XII.	Effect of back reflectors of the form ZnO/Al on short-circuit current density and quantum efficiency at 700 nm as a function of ZnO thickness.	33

SUMMARY

Objectives

The primary objective of this subcontract is to develop the technology for same bandgap, amorphous silicon tandem junction photovoltaic modules having an area of at least 900 cm^2 with the goal of achieving an aperture area efficiency of 9%. A further objective is to demonstrate modules that retain 95% of their power output under standard light soaking conditions.

Discussion

Our approach to the attainment of these objectives is based on the following distinctive technologies: a) in-house deposition of SiO_2/SnO_2:F onto soda lime glass by APCVD to provide a textured, transparent electrode, b) single chamber r.f. glow discharge deposition of the a-Si:H layers onto vertical substrates contained with high packing density in a "box carrier" to which the discharge is confined, c) sputter deposition of highly reflecting, ZnO-based back contacts, and d) laser scribing of the a-Si:H and electrodes with real-time scribe tracking to minimize area loss.

Continued development of single junction amorphous silicon was aggressively pursued as a proving ground for various optical enhancement schemes, new p-layers, and i-layer quality. The culmination of this effort was the measurement of a 1.05-cm^2 p-i-n cell at 11.3% efficiency. The high short-circuit current density (18 mA/cm^2) results from the use of an MgF_2 AR coating, a low-absorption p-layer, and a highly reflective back contact consisting of ZnO backed with Ag. The excellent fill factor for this 1 cm^2 cell (72%) is testimony to the high quality and good transport properties of the i-layer. The cell was isolated from a 1 ft^2 substrate coated in an a-Si:H deposition system capable of simultaneous deposition on 4 1-ft^2 substrates. Diborane was used as the p-layer dopant gas.

In a smaller research system, the development of high efficiency p-i-n cells was undertaken using trimethylboron (TMB) as the p-layer dopant gas. A study of the relationship between conductivity and Tauc gap for a-$Si_{1-x}C_x$:H p-layers using B_2H_6 and TMB as dopant sources showed that in the neighborhood of 2 eV bandgap, higher conductivities could be achieved using TMB. Even without a transitional i-layer (i_t), a cell efficiency of 10.5% has been attained using the TMB layer.

Our best tandem cell has an efficiency of 9.3%. The cell features a graded-index glass surface to eliminate front surface reflection, and a TiO_x interstack recombination layer to improve voltage and fill factor. The optimized second stack p and i_t layers differ somewhat from those of single junction devices. It maybe noted that all devices described in this summary employ carbon-graded p and i_t layers.

High quality amorphous silicon material layers and cells have also been produced in a new research deposition system intended for module development. This system is load-locked, and is designed to produce high purity layers with good thickness uniformity right up to the edges of the 1 ft^2 substrates. Extremely uniform photovoltaic performance was demonstrated across a 1 ft^2 substrate coated in this system.

Several studies of deposition uniformity have been conducted. Some possible sources of thickness variation across a large substrate are a) gas distribution effects, b) r.f. effects, and c) change of gas composition in the direction of flow. The last effect is particularly noticeable for a-$Si_{1-x}C_x$:H p-layers; it has been found that the spatial variation of H, C, and B concentrations in the deposited film along the direction of gas flow act in concert to increase bandgap and decrease conductivity. For example, it is possible to observe a change in p-layer conductivity from 3.4 x 10^{-5} S/cm to 3.0 x 10^{-7} S/cm over a gas flow distance of 25 inches. Based on these studies, the uniformity of both p and i layer properties have been improved.

New records have also been set for single and tandem junction modules of various sizes. The successful development of a process for incorporating back reflectors into 1 ft^2 modules, including critical annealing schedules, has allowed the attainment of an aperture area efficiency of 7.55% for a 1 ft^2 single junction module with a ZnO/Al back contact. This module has an aperture area of 873 cm^2 and generates 6.59 W. A new, high-precision X-Y table for laser patterning has allowed scribe related area losses to be reduced to 3%.

In the Eureka project, the application of many of the techniques mentioned above has resulted in the achievement of a world record power output for a monolithic thin film PV module of 74.4 W. This single junction module (approximately 155 cm x 79 cm) has an aperture area of 11,900 cm^2, generates 61 V open circuit, 1.85 A short circuit, and possesses the remarkable fill factor of 66%. The measurements were performed by SERI.

With tandem junction silicon, aperture area efficiencies of 7.17% and 6.42% have been achieved for 1 ft^2 and 1 x 3 ft^2 modules, corresponding to powers of 6.04 W and 16.4 W, respectively. These modules were metallized with Al; higher efficiencies are anticipated upon application of a back reflector.

In the all-important area of stability we have not made any attempt to better a previously announced achievement of only 11% power loss from an encapsulated 1 ft^2 tandem junction module during a period of over 140 days outdoor exposure. However, the following new results have been obtained. We have rigorously demonstrated, for example, that the introduction of a transitional i-layer does not impair stability, and that the initial gain in performance is retained. We have also demonstrated a small improvement in cell stability through a post-fabrication treatment consisting of multiple, intense light flashes followed by sufficient annealing. Finally, several experiments have indicated that long term stability can be improved by overcoating the SnO_2 with ZnO, but further work is necessary to understand the various factors at work.

Conclusions:

Performance data for single and tandem junction cells and modules are summarized in Table I. Good progress has been made in single junction technology, as evidenced by the performance of the 1.2 m^2 Eureka modules, 900 cm^2 modules with ZnO/Al reflectors, and 1 cm^2 cells with ZnO/Ag reflectors. However, additional efforts are required to realize corresponding advances in tandem junction cells and modules in order to improve stabilized efficiency. It is clear that improvements in the amorphous silicon layers will continue to be a major factor in achieving these goals, and that techniques for obtaining deposition uniformity over large areas, and for obtaining novel doped layers with higher transparency and conductivity, must be brought into the mainstream. In this context, initial results with trimethylboron (TMB) as a p-type dopant source for $a\text{-}Si_{1-x}C_x$:H window layers have been very encouraging.

Table I: Performance of amorphous silicon cells and modules (single and tandem junction)

Device type	Power (W)	Area (cm^2)	Efficiency (%)	V_{oc} (V)	J_{sc} or I_{sc} (mA/cm^2 or mA)	FF (%)	AR	Metallization	Measured at
1J cell	-	1.05	11.3	0.854	18.3	72.2	MgF_2	ZnO/Ag	Chronar
1J cell (TMB, no I_1)	-	0.072	10.5	0.823	17.4	73.7	MgF_2	ZnO/Ag	Chronar
1J module (1x1)	6.59	873	7.55	24.2	404	67.0	-	ZnO/Al	SERI
1J module (Eureka)	74.4	11,900	6.23	61.0	1848	66.0	-	Al	SERI
2J cell	-	0.08	9.30	1.65	7.47	75.6	G.I.	Al	Chronar
2J cell	-	1.00	8.70	1.64	7.41	71.6	-	Al	Chronar
2J module (1x1)	6.04	842	7.17	48.3	189	66.1	-	Al	Chronar
2J module (1x3)	16.4	2,555	6.42	46.7	548	64.1	-	Al	SERI

Notes: J_{sc} given for cells, I_{sc} given for modules
G.I. denotes graded-index glass

Module performance is still diminished relative to cell performance by problems related to patterning and to defects of various origin. The underlying causes must be understood and brought under control. With the emphasis on stabilized efficiency and increased outdoor testing, encapsulation issues must be faced within these research programs, and encapsulation materials and processes developed so that environmental effects do not contribute to power loss. Until this is accomplished, it will remain difficult to separate long term power loss observed in the field into contributions from the Staebler-Wronski effect and/or possible materials problems at cell interfaces. Concerning the latter issue, the demonstration of improved long term stability through the use of ZnO as a substrate for a-Si:H deposition (rather than SnO_2) is potentially of far-reaching consequence.

SECTION 1.0

INTRODUCTION

In completing the third phase of research on stable, large area amorphous silicon based modules, we have set new efficiency records for both cells and submodules of various sizes (see Table 1). A major factor has been the development using small area cells of highly reflective ZnO-based contacts, and their successful application (involving critical laser scribing and annealing steps) to submodules.

The research program has been organized into three areas, and this document adopts that division for reporting purposes. An outline of the objectives in each area is as follows:

Semiconductor Materials and Small Area Cells:

The objectives here include the deposition of amorphous silicon materials over large areas, the optimization of these materials as guided by physical, chemical, electrical and optical characterization, and the optimization of the efficiency and stability of small area p-i-n and p-i-n/p-i-n cells.

Non-Semiconductor Materials:

Here the objectives are the deposition of front and back contact materials (transparent conductors and metallization) over large areas, the development of advanced back reflectors, minimization of optical losses, and study of the thermal stability of the associated materials and interfaces.

Submodules:

The objectives here are the fabrication and optimization of large area interconnected devices on a monolithic substrate. This includes investigation of submodule configurations and patterning approaches, increase of active area, defect analysis, and a comparison of the light soak behavior of single and tandem junction submodules.

Research performed during the first half of Phase III is described in much greater detail in the semi-annual report [1].

SECTION 2.0

SEMICONDUCTOR MATERIALS AND SMALL AREA CELLS

2.1 DEPOSITION OF AMORPHOUS SILICON

Hydrogenated amorphous silicon (a-Si:H) was prepared by r.f. glow discharge decomposition of either SiH_4 or a SiH_4/H_2 mixture in various deposition systems. Regardless of layer type or sequence, all layers were prepared in a single chamber. Four deposition systems were employed during the second half of Phase III of the subcontract as a source of a-Si:H. Three of the systems are research systems, while the fourth (Eureka) system is part of a line being readied for manufacturing. These systems may be briefly described as follows:

- The D1 system, holding four 1 ft x 1 ft (929 cm^2) vertical substrates
- The Eureka system, holding forty-eight 31 inch x 61 inch (1.22 m^2) vertical substrates
- The B system, holding one 2 inch x 2 inch (26 cm^2) horizontal substrate
- The D2 system with inlet and outlet load locks, and holding four 1 ft x 1 ft (929 cm^2) vertical substrates.

In all cases the discharge is confined within an inner box positioned within the actual vacuum chamber. In three of the systems the inner box (or box carrier) holds multiple substrates oriented vertically with high packing density. The basic arrangement and its advantageous features have been described in earlier publications [2, 3, 4].

Our research strategy concerning these four systems may be described briefly as follows. The D1 system has traditionally been our workhorse deposition system, and has in fact produced the highest efficiency devices. In common with Chronar's manufacturing technology, it utilizes the box carrier concept in order that research results stand a reasonable chance of being applicable to the real world. The recently-constructed D2 system was designed to provide a comparison of the efficiency and stability of cells prepared in a load-locked system versus those prepared in the non-load locked D1 system. It was also designed to give uniform deposition of a-Si:H right up to the edges of the 1 ft^2 substrates, a feature that is desirable for module fabrication. The small area B system is employed as a flexible, high throughput system for initial development of new concepts and layers. Finally, the Eureka system has been employed in this program as a convenient source of amorphous silicon for back reflector development, and for stability studies.

High quality i-layers (as documented in section 2.2 below) are routinely produced in all four systems described above. That dopant cross-contamination can be successfully controlled

in single chamber deposition systems of appropriate design is evident from the production of p-i-n devices having fill factors greater than 0.75 in three of the above systems (D1, Eureka, B). The fourth system (D2) has produced fill factors of 0.72, limited we believe only by insufficient optimization. From the point of view of manufacturing it is indeed fortunate that cross contamination can be controlled in single chamber systems, for this allows decisive advantages in terms of equipment cost, reliability, ease of maintenance, and throughput.

2.1.1 Features of the D2 - system

A block diagram of the D2-system is shown in Fig. 1. It consists of three in-line vacuum chambers (entry, deposition, and exit chambers) with 6" x 22" gate valves isolating the central deposition chamber. This load-lock arrangement prevents the deposition chamber from being exposed to the atmosphere.

Infrared heating of the inner box in a gaseous ambient is provided for in the entry chamber, and the entry and exit chambers are pumped with 400 l/s turbo-molecular pumps. The box carrier is transported using motor-driven rollers, and is designed to have minimal cross-talk between the plasma and chamber volumes. Separate p, i, and n gas manifolds have been installed, and steady-state flows can be established in all manifold lines prior to introduction of gas into the deposition chamber. This feature, together with the use of an automatic pressure control valve, minimizes the time dopant gases are in the chamber prior to film growth.

2.2 I-LAYER PROPERTIES

2.2.1 Long Diffusion Length of D1-system Material

The excellent transport properties of D1 system a-Si:H material have been confirmed by both diffusion length and collection data. Thus, using the steady state photocarrier grating (SSPG) technique, an ambipolar diffusion length of 2200 Å was found for a standard i-layer [5]. This is roughly equal to $\sqrt{2}$ x the minority carrier (hole) diffusion length. Direct measurement of the electron and hole mobility-lifeline ($\mu\tau$) products in a 10 μm thick p-i-n structure gave $\mu_e\tau_e = 3.0 \times 10^{-7}$ cm^2 V^{-1} and $\mu_n\tau_n = 2.2 \times 10^{-8}$ cm^2 V^{-1} [5]. These parameters were determined from charge collection using strongly absorbed light.

The hole $\mu\tau$ product determined in this fashion is consistent with the ambipolar diffusion length determined by the SSPG technique. It is of interest that the intensity dependence of the ambipolar diffusion length can be written $L \propto F^{-s}$ with s = 0.2 for intrinsic a-Si:H, but for an i-layer deposited after a p-layer (i.e. a p-i structure) s = 0.14, a result which is advantageous for p-i-n solar cells [7]. Further details of the

Figure 1. Block diagram of the D2 a-Si:H deposition system

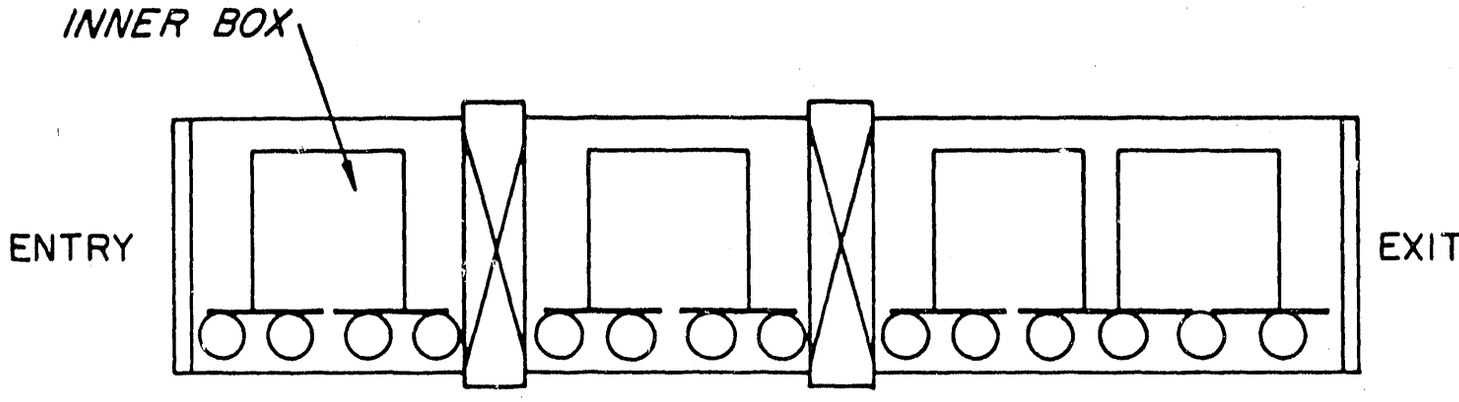

above techniques, together with a demonstration of the connection between i-layer defect density and cell fill factor using thermally stimulated currents and current DLTS, can be found in earlier subcontract reports [8,9].

2.2.2 Opto-electronic Properties of D2 and B System Material

The new D2 system also produces i-layers of high quality. Analysis of sample D2-4RW, which was an i-layer of thickness 0.54 μm deposited on Corning 7059 glass, gave the properties listed in Table II below.

Table II. Opto-electronic properties of D2-system and B system i-layers

Property	**D2-system**	**B-system**	**Unit**
Deposition rate	1.0	-	A/s
Band gap	1.76	1.76	eV
Dark conductivity	9.1×10^{-11}	1.5×10^{-10}	$(\text{ohm cm})^{-1}$
Photo-conductivity (at AM1)	1.4×10^{-4}	9.1×10^{-5}	$(\text{ohm cm})^{-1}$
Photo/dark ratio	1.5×10^{6}	6.1×10^{5}	-
Gamma (see Fig 3 & 4)	0.87	0.89	-
Alpha (600 nm)	4.2×10^{4}	-	cm^{-1}
Activation energy	-	0.81	eV

Some of the relevant deposition conditions for the D2-system i-layer were: Substrate temp 183°C, base pressure 9.8×10^{-6} torr, deposition pressure 500 mTorr, silane flow 12 sccm, hydrogen flow 25 sccm, net RF power 12-14 W, time 90 min. A thickness map for the right wall plate is given in Fig. 2. The center of all four plates from this run yielded a film thickness of 5400 A.

Also shown in Table II are the properties of a typical B-system i-layer (sample B-145, thickness 0.425 μm). Independent optimization of this system resulted in i-layer properties very similar to those produced in the D1 system. This can be further seen in Figs. 3 and 4, which are log-log plots of photoconductivity versus light intensity for the two i-layers. Writing $\sigma p \propto I^{\gamma}$ gives γ values of 0.87 and 0.89 for the two films. Both films had a bandgap of 1.76 eV, and their dark and (1 sun) photoconductivities were similar. An activation energy plot of the dark conductivity versus temperature for sample B-145 is shown in Fig. 5. The slope of the plot gives an activation energy of 0.81 eV. One missing piece of information is the ambipolar diffusion length, which has not yet been measured for either D2 or B system material. Directions for further i-layer development are discussed below.

2.2.3 Directions for Further I-layer Development

We have seen in section 2.2.1 that excellent transport properties can be obtained for conventional, as-deposited intrinsic a-Si:H. Nevertheless, for solar cell applications, it

Figure 2. Thickness map for a-Si:H deposited on a 1 ft^2 substrate in the D2-system

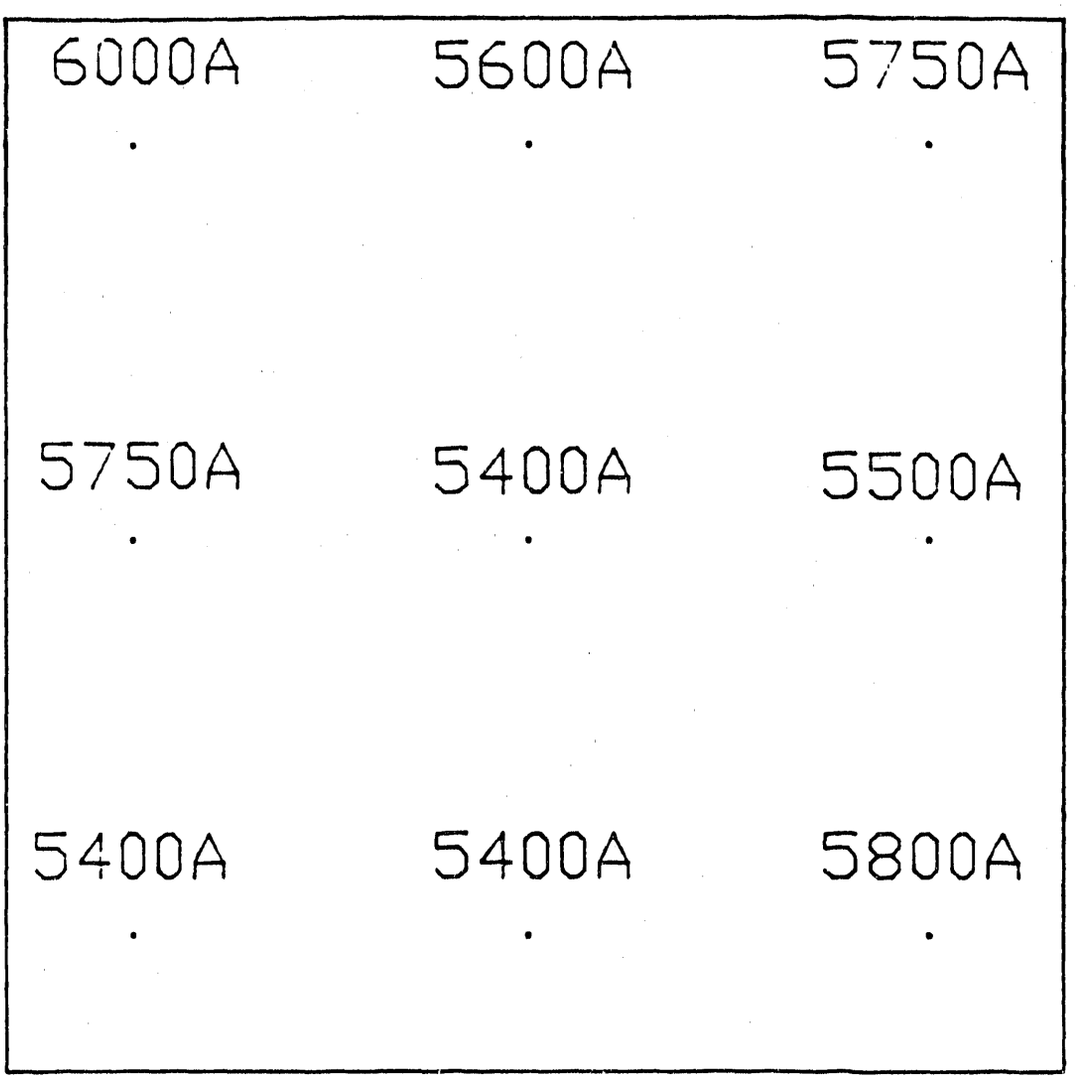

Figure 3. Log - log plot of photoconductivity versus light intensity for a D2-system i-layer

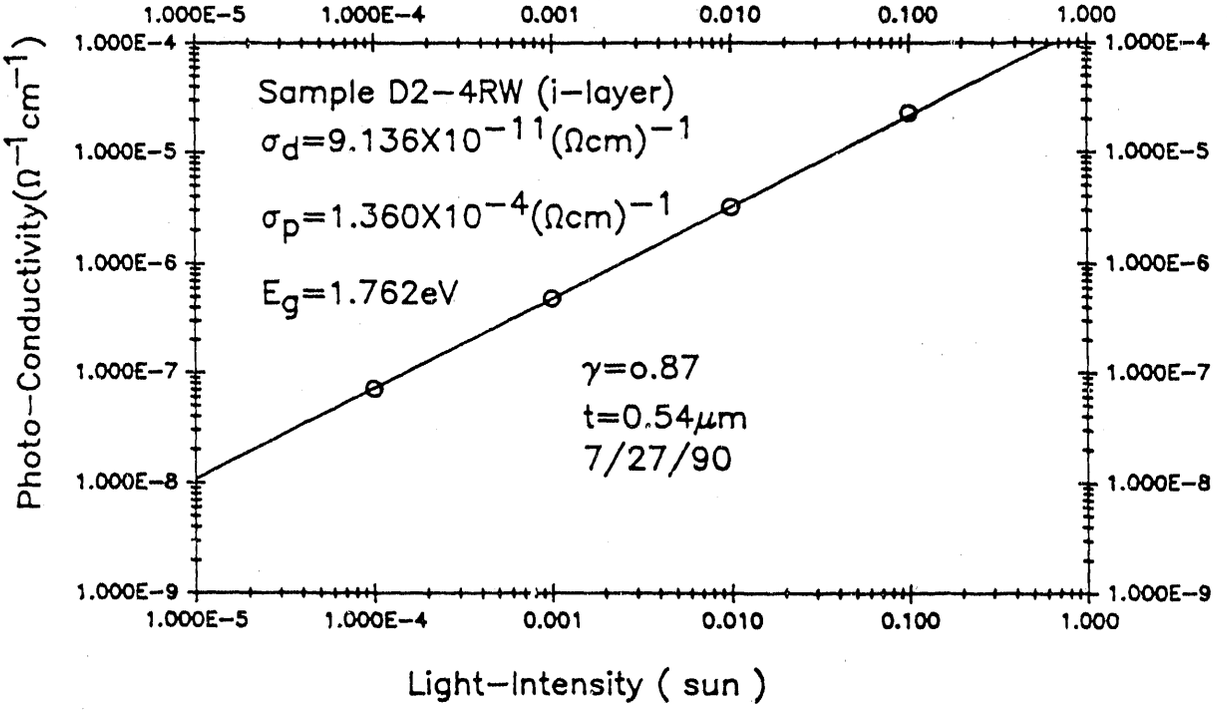

Figure 4. Log - log plot of photoconductivity versus light intensity for a B-system i-layer

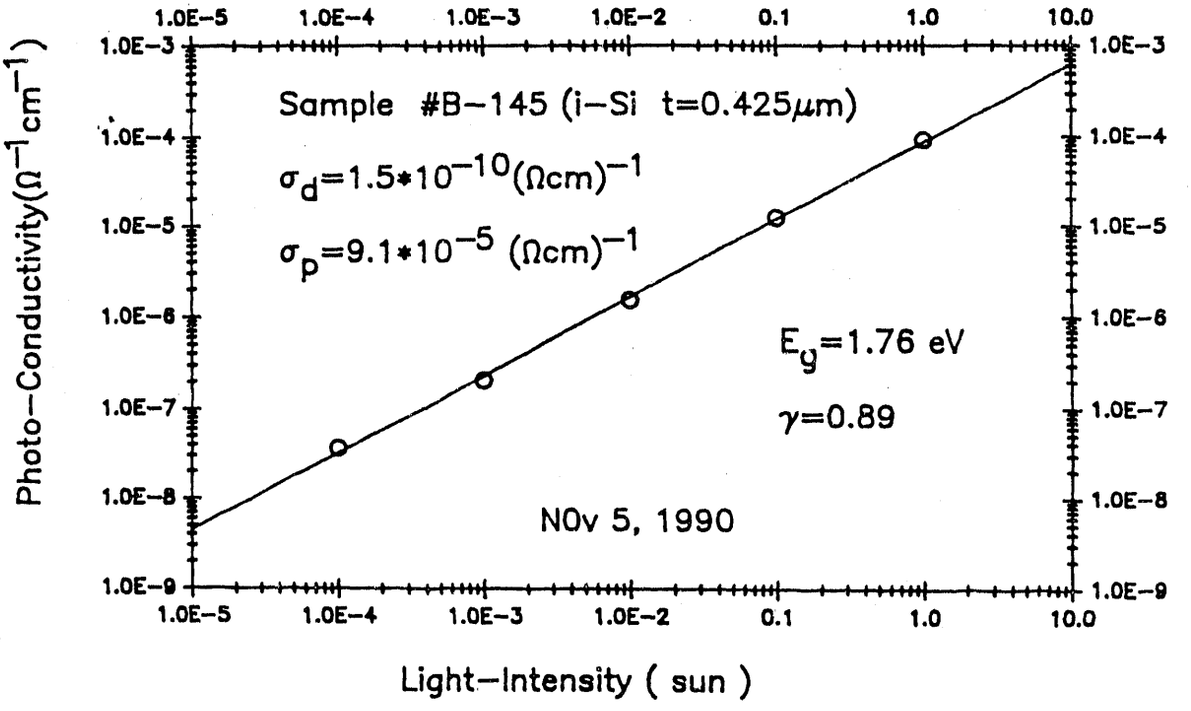

Figure 5. Dark conductivity versus 1/T (activation energy plot) for the B-system i-layer of Fig. 4.

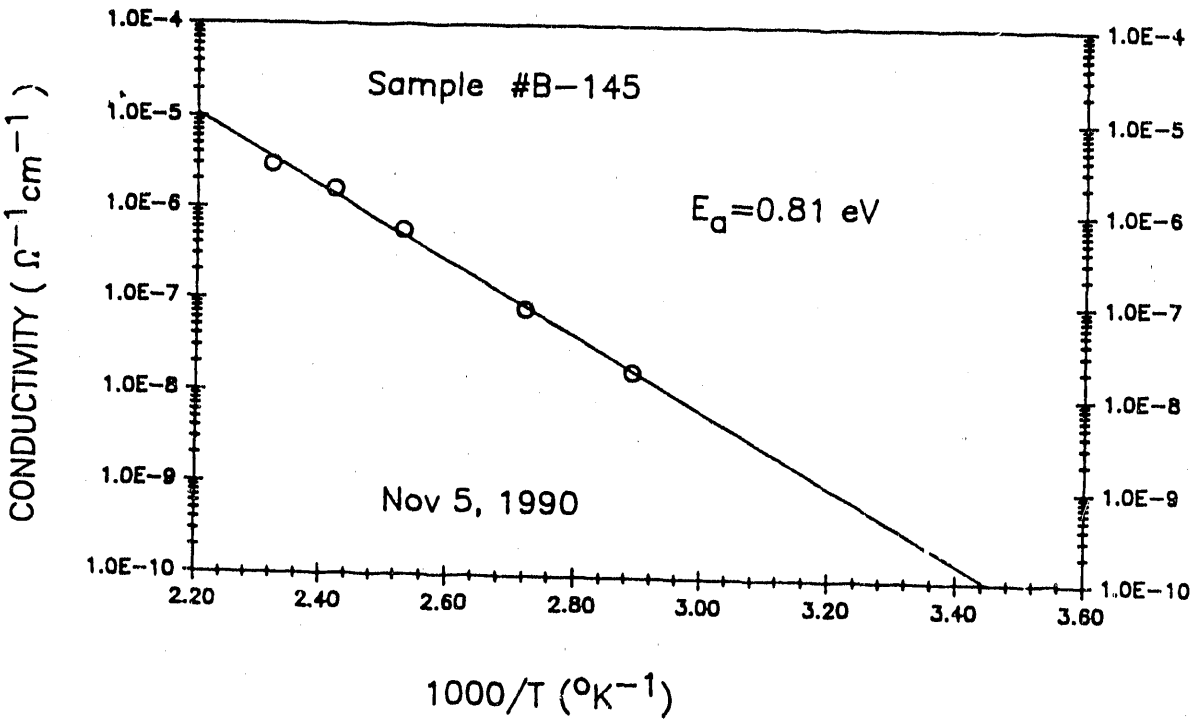

would be desirable to improve two other properties of a-Si:H i-layers, namely, optical absorption and photostability.

It is generally thought that use of a higher substrate temperature, Ts, during a-Si:H deposition is an effective method to enhance optical absorption and to reduce light-induced degradation. However, until recently, it appeared that transport properties were impaired at high Ts. The recent work of Nakano et al. shows that this need not be the case, provided an ultra-high vacuum chamber is employed and degradation of the p-layer and p-i interface can be prevented [10].

Another possible route to improved stability is to prepare a-Si:H i-layers at extremely low deposition rates and low Ts, possibly in conjunction with a further means to promote the rejection of excess hydrogen at the surface of the growing film.

2.2.3.1 Enhanced Optical Absorption

By using extremely low RF power density (down to 3 mW/cm^2), low pressure (down to 100 mTorr), and slightly increased substrate temperature (from 200 to 230°C) we have demonstrated i-layer with enhanced optical absorption while maintaining superior electronic quality. This work was performed in the B-system. Use of this material in p-i-n devices resulted in significant enhancement of J_{sc}, while efficiency matched the best low temperature devices.

2.3 P-LAYER RESEARCH

In order to fabricate large area a-Si:H modules of the highest performance it is of course desirable that the p-layer should possess uniform properties over the entire module surface. In practice some variation may be tolerated, provided that the transmission and conductivity do not fall below certain values. We describe below two studies relating to these issues of uniformity. In these studies diborane was employed as the p-type dopant source. However, it is known that diborane catalyzes the decomposition of silanes at relatively low temperatures [11], and that the diborane concentration in gas cylinders containing diborane diluted in silane decreases with time as measured by gas chromatography. For these reasons we have also investigated the use of the more stable gas trimethylboron, $B(CH_3)_3$ or TMB, as an alternative source of boron. This too is described below.

2.3.1 Variation of P-layer Properties in Direction of Gas Flow

It is widely appreciated that in a silane-based discharge the gas composition changes in the direction of gas flow as concentrations of stable molecules such as disilane and hydrogen are built up through secondary reactions in the gas. We have found that such effects are particularly pronounced in the deposition of a-$Si_{1-x}C_x$:H p-layers from mixtures of silane, methane, and diborane. In particular, we have shown that the spatial variation of H, C, and B concentrations in the deposited film along the direction of gas flow act in concert to

increase bandgap and decrease conductivity. For example, it is possible to observe a change in p-layer conductivity from 3.4 x 10^{-5} S/cm to 3.0 x 10^{-7} S/cm over a gas flow distance of 25 inches, and a corresponding increase in bandgap from 1.90 eV to 1.99 eV. Further details of the change in p-layer properties in the direction of gas flow are shown in Table III.

Table III

Variation of a-$Si_{1-x}C_x$:H p-layer properties as a function of position in the direction of gas flow; the gas mixture consists of silane, methane, and diborane.

Position (inches)	Thickness (Å)	Bandgap (eV)	Conductivity (S/cm)	Absorption at 400 nm (cm^{-1})	[C] (cm^{-3})	[B] (cm^{-3})	[H] (%)
3	1010	1.90	3.4×10^{-5}	4.5×10^{5}	3.0×10^{21}	6.9×10^{20}	41
15.5	980	1.94	6.6×10^{-6}	3.7×10^{5}	-	-	-
28	800	1.99	3.0×10^{-7}	3.4×10^{5}	3.8×10^{21}	2.9×10^{20}	54

It was further demonstrated that the variation in p-layer properties were responsible for an observed variation in p-i-n device behavior in the direction of gas flow. For it had earlier been noticed that small area devices fabricated near the gas inlet manifold were of lower efficiency (7.8%) than those fabricated near the gas outlet manifold (8.3%). Near the inlet, J_{sc} and FF were 13.0 mA/cm^2 and 74.1%, respectively, while near the outlet the corresponding figures were 14.6 mA/cm^2 and 69.1%. Spectral response measurements revealed that the devices fabricated 28" downstream (i.e. near the gas outlet) possessed a much higher blue response. This is shown in Fig. 6. It thus becomes clear that the larger bandgap (and increased short wavelength transparency) of the p-layer deposited from the downstream gas mixture (i.e. the mixture resulting from the action of the discharge over a 28" distance) is responsible for the higher blue response and hence higher J_{sc} of the downstream device, while the decreased conductivity of the p-layer is responsible for the lower FF of the downstream device. (Other experiments demonstrated that the lower FF was not due to inferior i-layer quality).

2.3.2 Influence of Diborane Concentration on Cell Uniformity

We have discovered that the concentration of diborane used in the p-layer gas mixture can have a major effect on the spatial uniformity of the conversion efficiency of p-i-n devices. This work was performed in a glow discharge system handling 1 ft^2 substrates.

Figure 6. Spatial variation of the spectral response and overall photovoltaic parameters of p-i-n cells caused by the variation of their p-layer composition in the direction of gas flow

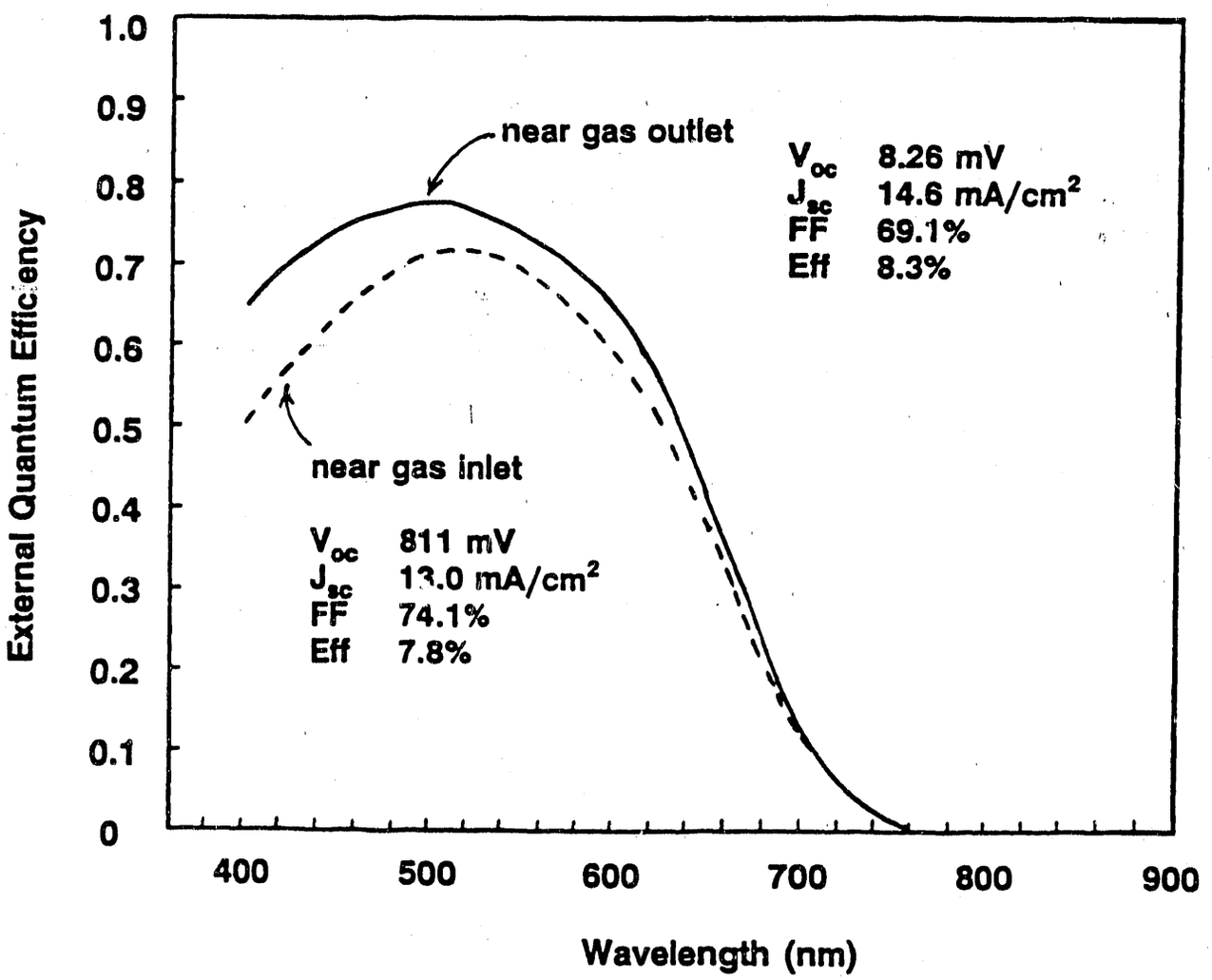

he following experiments suffice to illustrate the above result. Using p-layer gas mixtures consisting of silane, methane, diborane, and helium, two p-i-n device runs were performed that were identical in all respects except for the p-layers. The first run (DL585) was performed according to a standard prescription, while in the second run (DL591) the flow rate of the p-layer dopant gas (diborane diluted in helium) was halved. The total helium flow was left unchanged by addition of helium from a cylinder of pure helium plumbed in for that purpose. In this way the total gas flow rates for the p-layers in these run were kept essentially equal. On each of the 1 ft^2 substrates an array of 16 diagnostic cells was formed in order to sample all regions of the amorphous silicon. The spatial distribution of cell efficiencies was found to be drastically different in the two runs, with the second run (DL591) exhibiting much better uniformity. Both runs achieved roughly the same peak efficiencies, but the second run did not suffer from large drops in efficiency near the edges (and especially the corners) of the substrate. A summary of the data is given in Table IV, from which it can be seen that the halving of the diborane flow increased in average diagnostic cell efficiency from 8.0% to 9.0% and greatly reduced the standard deviation from 0.9% to 0.4%.

Table IV Distribution of cell efficiency across a 1 ft^2 substrate as a function of diborane concentration in p-layer gas mixture.

Run#	Flow rates of p-layer gases (sccm)				cell efficiencies(%)			
	SiH_4	CH_4	B_2H_6	He	low	high	average	S.D.
DL585	13.8	14.4	1.25	40	5.8	9.3	8.0	0.9
DL591	13.8	14.4	0.65	41	8.1	9.4	9.0	0.4

Spectral response data taken on diagnostic cells along a line in the direction of gas flow proved quite interesting. In the second run (lower diborane concentration) the general behavior described in section 2.3.1 above was observed, namely an increase in integrated current in the direction of gas flow (the increase resulting from higher blue response), and a decrease in QE(0.6V)/QE(0V). These observations were consistent with changes in J-V parameters, namely J_{sc} = 15.1 mA/cm^2 and FF = 71% near the gas inlet, and J_{sc} = 15.6 mA/cm^2 and FF = 67% near the gas outlet. As explained in section 2.3.1, these changes are caused by changes in p-layer transparency and conductivity. In contrast to this, the first run (higher diborane concentration) exhibited anomalous behavior. High cell efficiencies were obtained only in the center region of the substrate, with low values of J_{sc}, FF, integrated current, and QE(0.6V)/QE(0V) being obtained particularly near the gas inlet (e.g. J_{sc} = 13.3 mA/cm^2, FF = 63%), and to a lesser extent near the gas outlet. In both of

these regions plots of QE(0.6V)/QE(0V) versus wavelength dipped markedly at short wavelengths, implying a weak field near the p-i interface and/or a slightly p-type i-layer. It would therefore appear that in the first run residual boron is being incorporated in at least the initial part of the i-layer, and, near the edges of the plate, in sufficient quantities to degrade the performance of the p-i-n device. This residual boron effect masks the variation in p-layer properties described above.

In conclusion, we have shown in the last two sections that variations in p-layer properties and/or residual boron can be major sources of spatial non-uniformity of p-i-n cells and are liable to dominate the small effects resulting purely from variations in the physical thickness of the layers.

2.3.3 Use of Trimethylboron as a P-type Dopant Source

We have investigated the use of trimethylboron, $B(CH_3)_3$ or TMB, in place of diborane as a p-type dopant gas for amorphous silicon carbide window layers. This work was prompted by the reported achievement of superior window layers using TMB by Tarui et al. [12], and by the work of Zongyan et al. who found much lower levels of boron cross-contamination using TMB (as opposed to diborane) owing to the greater stability of TMB [13].

Our own work has employed both H_2 and He as diluents. In one deposition system, using TMB in H_2, the following properties were obtained for amorphous silicon carbide p-layers prepared at 200°C: optical gap 2.0 eV, dark conductivity 6×10^{-7} ohm^{-1} cm^{-1}, activation energy 0.45 eV. Using this p-layer, the following device results were obtained: V_{oc} = 860 mV, J_{sc} = 14.5 mA/cm^2 (Al metallization, no AR coating) FF= 68%, Efficiency = 8.5% (run DL525). These results are somewhat inferior to those obtained with diborane-derived p-layers. It is worth remarking, however, that the use of TMB enabled a lower ratio of CH_4 to SiH_4 to be employed than that required by diborane in order to achieve an adequately wide bandgap. This suggests that TMB is a more efficient dopant than diborane, and causes less bandgap reduction. A similar observation has been made by Catalano et al. [14].

Further development of TMB p-layers was pursued in another deposition system, with the following results: optical gap 2.0 eV, dark conductivity 6×10^{-6} ohm^{-1} cm^{-1}, activation energy 0.46 eV. An even lower CH_4/SiH_4 ratio was employed. Using this p-layer in an optically-enhanced device, but without using a transitional i-layer, an efficiency of 10.5% was obtained. (V_{oc} = 823 mV, J_{sc} = 17.4 mA/cm^2, FF = 73.7%, see section 2.4). The relationship between dark conductivity and optical gap that we found using either diborane or TMB as the dopant source in amorphous silicon carbide window layers is shown in Fig. 7. From this data we can conclude that the TMB p-layer is superior to the diborane p-layer.

Figure 7. Dark conductivity versus bandgap for a-$Si_{1-x}C_x$:H p-layers doped using either diborane or trimethylboron

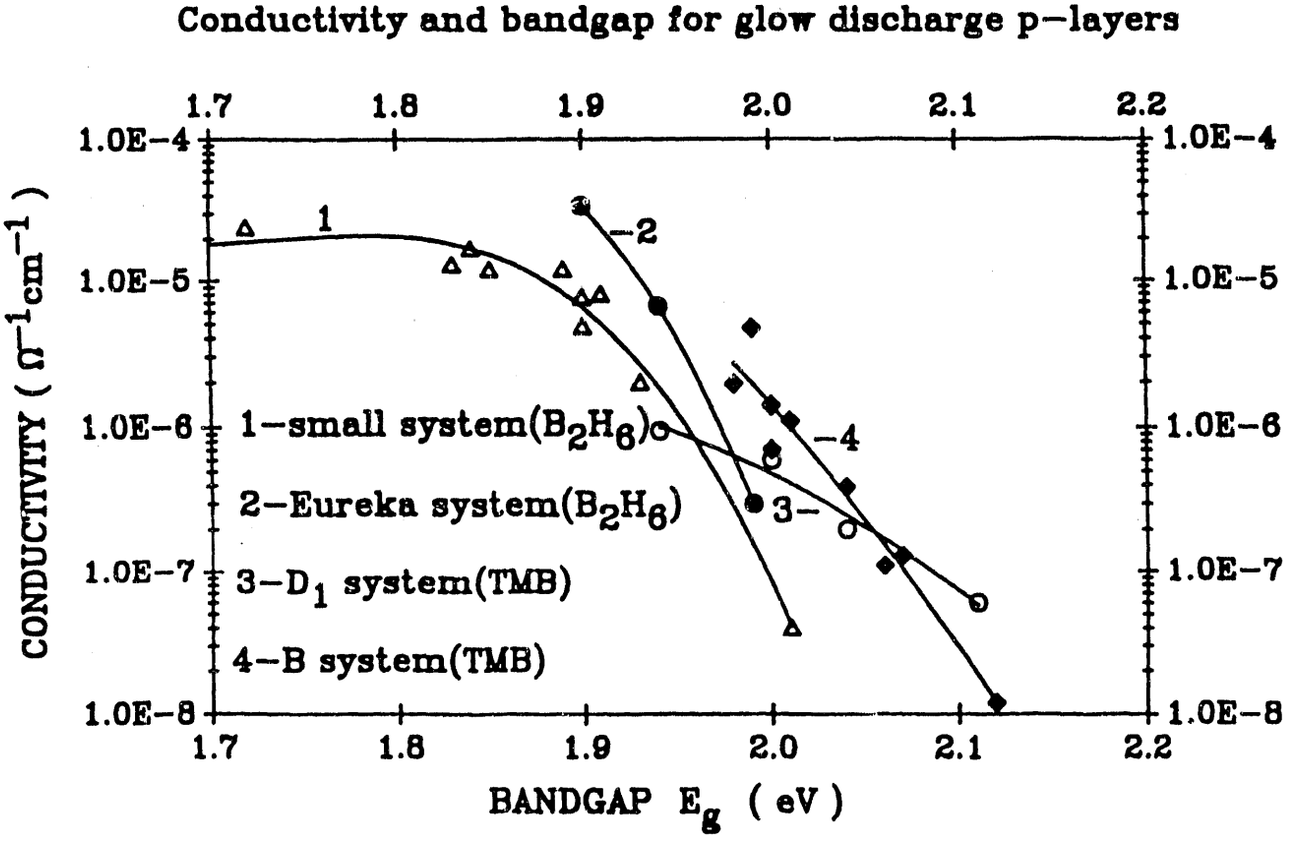

2.4 HIGH EFFICIENCY SINGLE JUNCTION CELLS

The continued development of single-junction amorphous silicon devices is being aggressively pursued as a proving ground for various optical enhancement schemes, new p-layers, and i-layer quality. This section describes the integration of several new elements into single-junction devices, the resulting performance of such devices, and plans for further increasing their efficiency.

2.4.1 Cells with TMB P-layers

One line of research has employed TMB exclusively as the dopant gas for p-layers. A cell efficiency of 10.5% has been obtained for a 0.072 cm^2 device with the structure:

MgF_2/soda lime glass/SiO_2/SnO_2:F/p(a-SiC)-i(a-Si)-n(a-Si)/ZnO:Al/Ag

The J-V curve of this device is shown in Fig. 8. Substantial increases in V_{oc} and J_{sc} are anticipated once a transitional i-layer is introduced.

2.4.2 Cells with Diborane P-layers

A second line of research currently employs diborane as the p-layer dopant gas. Here a 1.05 cm^2 cell efficiency of 11.3% has been achieved using the structure:

MgF_2/soda lime glass/SiO_2/SnO_2:F/p(a-SiC)-i_t(a-SiC)-i(a-Si)-n(a-Si)/ZnO:Al/Ag

The individual photovoltaic parameters of the cell were: V_{oc} = 854 mV, J_{sc} = 18.3 mA/cm^2, FF = 72.2%, and its J-V curve is shown in Fig. 9.

Critical to this achievement were the development of the following cell elements:

- MgF_2 AR coating
- SiO_2/SnO_2:F (granular, 8 ohms/square)
- C-graded p and i_t layers
- high quality i-layer (dot fill factors up to 0.75)
- sputtered ZnO:Al/Ag back reflector.

Figure 10 shows the J-V curve obtained by SERI for a 1.06 cm^2 cell having a similar structure, confirming that efficiencies in excess of 10% are obtained. At the time of writing, work is underway to attempt confirmation of the 11% value.

Figure 8. J-V curve for a 10.5% cell (area 0.0 F_2 cm^2) employing a TMB p-layer, ZnO/Ag reflector, but no transitional i-layer

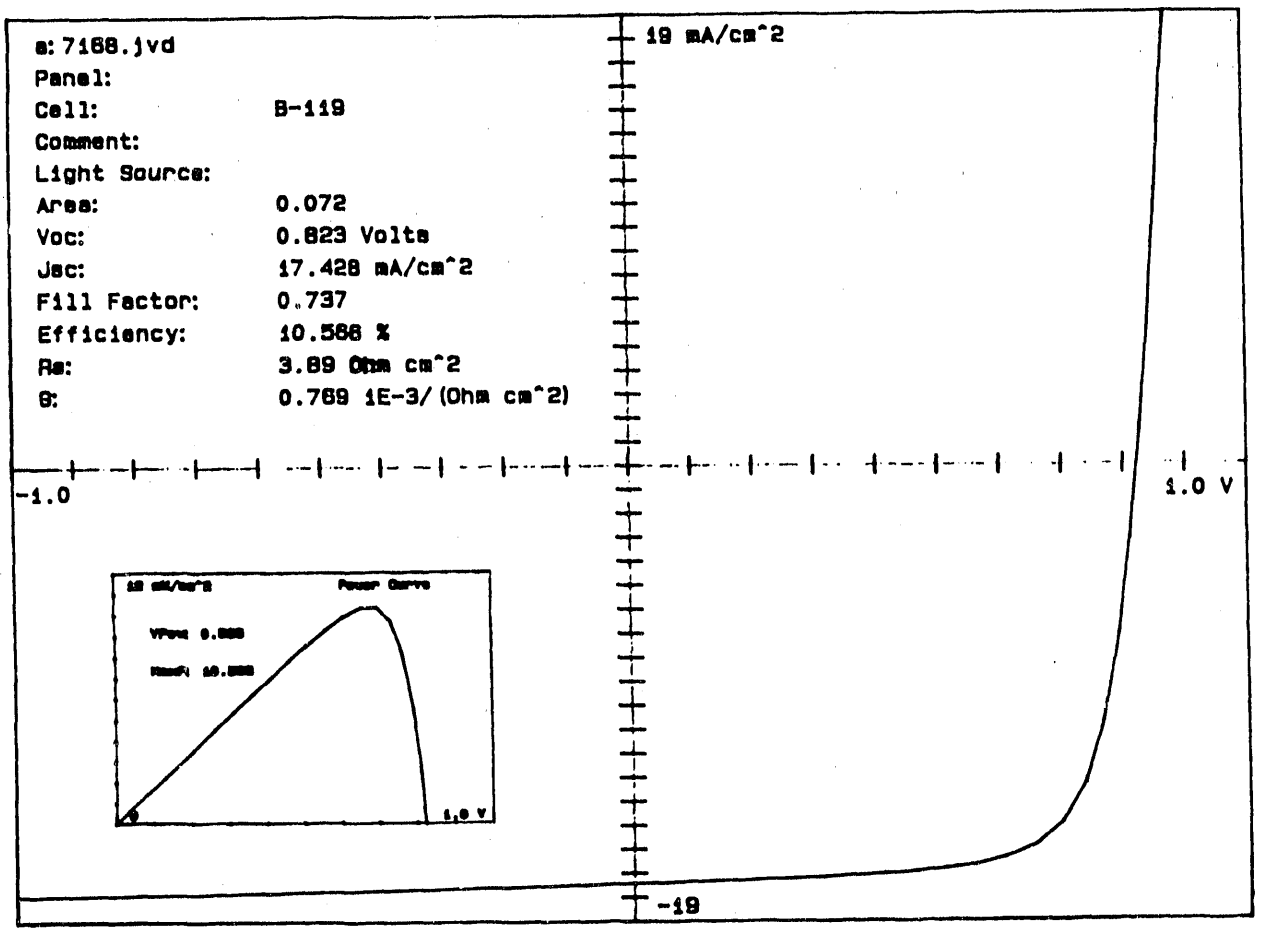

Figure 9. J-V curve for an 11.3% cell (area 1.05 cm^2) employing a diborane p-layer and ZnO/Ag reflector

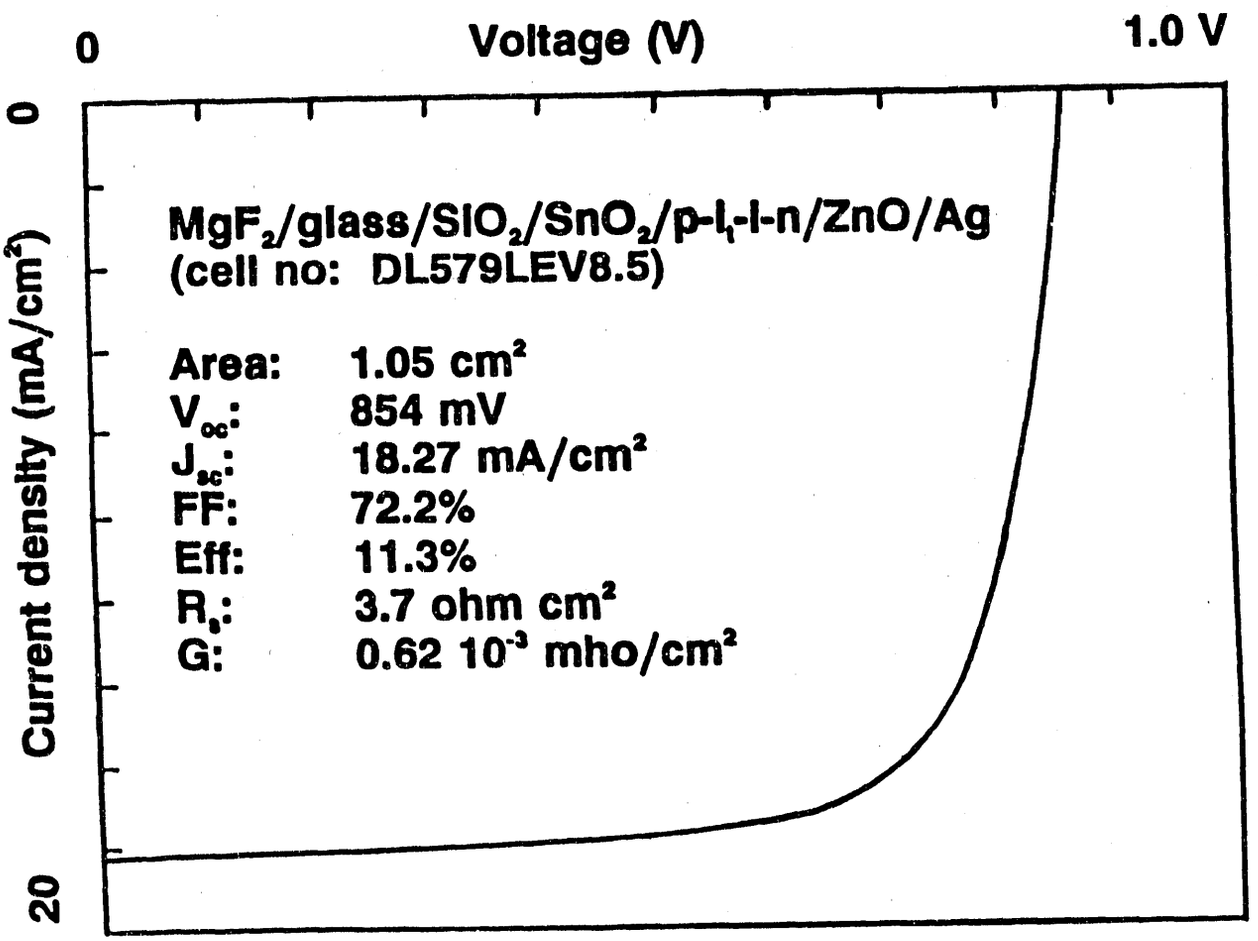

Figure 10. J-V curve obtained by SERI for a cell having the structure defined in Fig. 9.

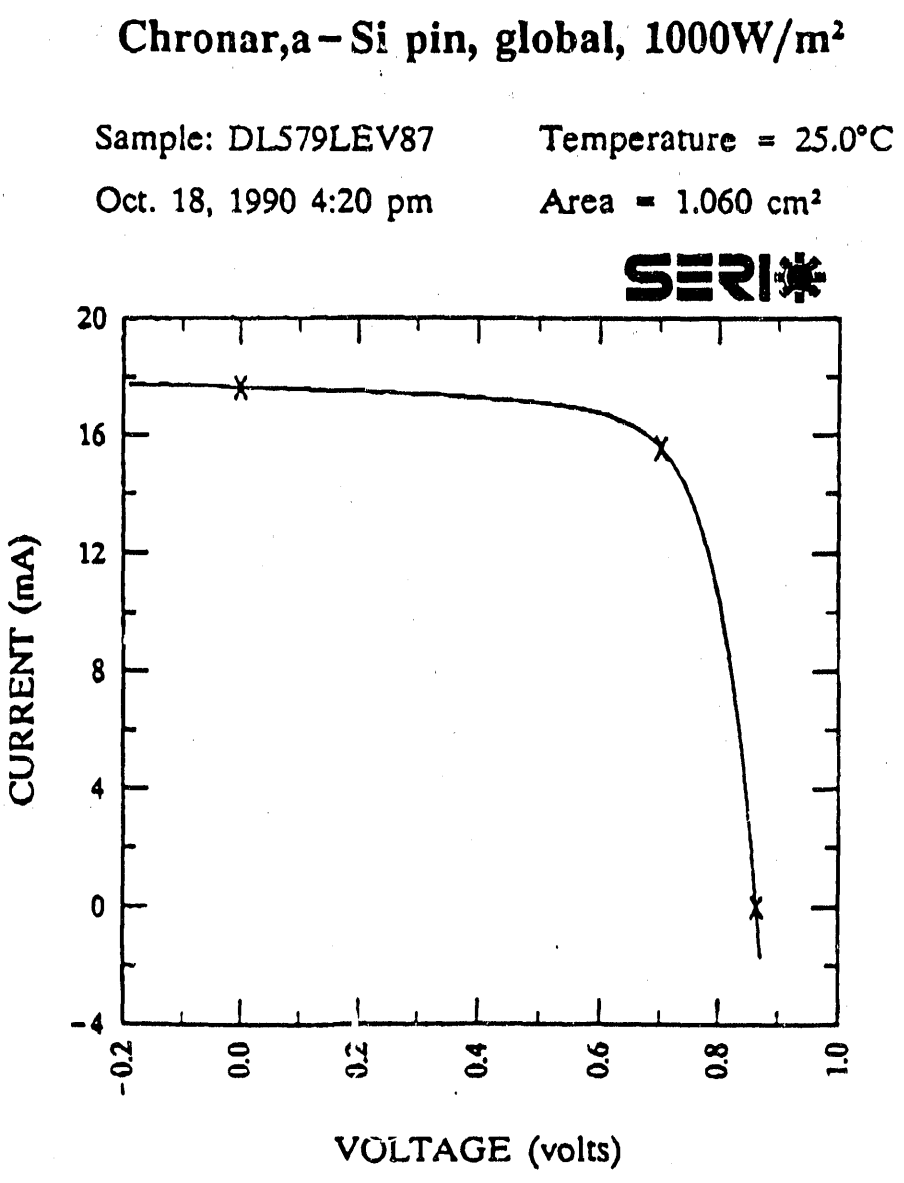

V_{oc} = 0.8039 volts
I_{sc} = 17.66 mA
J_{sc} = 16.66 mA/cm²
P_{max} = 10.94 mW
Fill factor = 71.72 %
I_{max} = 15.59 mA
Efficiency = 10.3 %
V_{max} = 0.7018 V

ttention is drawn to the fact that the cells described in this section were prepared on production-grade tin oxide deposited on 3 mm thick soda lime glass. Such glass possesses signigicant absorption at longer wavelengths. For example, at 700 nm we measure a transmission of 80% for tin oxide on soda lime glass, compared to 88% for similar tin oxide on 1 mm thick Corning 7059 glass.

A simple calculation of the estimated gain in J_{sc} through adoption of a Corning 7059 glass substrate yields about 0.5 mA/cm^2. Further gains in performance can be obtained through adoption and optimization of TMB p-layers (where appropriate), reduction of I^2R losses in the tin oxide through application of a grid, use of zinc oxide as a substrate, development of a wide gap (low index) n-layer and an improved reflectivity of the ZnO/Ag back contact. We are confident that the future use of these techniques will enable us to achieve an efficiency in excess of 12%.

2.4.3 Cells from the New D2-system

Cells produced in the new D2 system that was recently brought into operation have not yet matched those produced in the D1 system with regard to either efficiency or run-to-run reproducibility. The following data compares the photovoltaic parameters of the best 0.1 cm^2 cell obtained in each of the systems; the data are for cells without optical enhancement, i.e. with standard Al metallization and no AR coating:

	V_{oc} (mV)	J_{sc} mA/cm^2)	FF (%)	Eff (%)
D1	871	16.4	71.5	10.2
D2	855	14.6	71.2	8.9

On the other hand, truly excellent spatial uniformity has already been demonstrated in the D2-system. Thus, for arrays of 16 dots formed on 1 ft^2 substrates, a standard deviation of cell efficiency of 0.4% can be obtained in the D1 system, while a standard deviation of 0.15% has been obtained in the D2 system. It is gratifying that this aspect of the D2-system design has been vindicated.

2.5 TANDEM JUNCTION CELLS

The motivation for pursuing the more complicated tandem junction (p-i-n/p-i-n) structure is, of course, the achievement of a higher stabilized efficiency [15, 16]. The J-V curve of our best (9.3%) tandem junction cell is shown in Fig. 11. The cell features a graded-index glass surface to eliminate front surface reflection, and an 80Å TiO_x interstack recombination layer to improve voltage and fill factor [15, 16]. The optimized second stack p and i_t layers differ somewhat from those of single junction devices. The cell of Fig. 11 employed Al metallization. While we have not yet produced a record

Figure 11. J-V curve for 9.3% tandem junction cell with TiO_x interstack recombination layer

EMPLOYS:
graded-index AR glass
C-graded p-layers
SIC transitional i-layers
TIO_x inter-stack layer

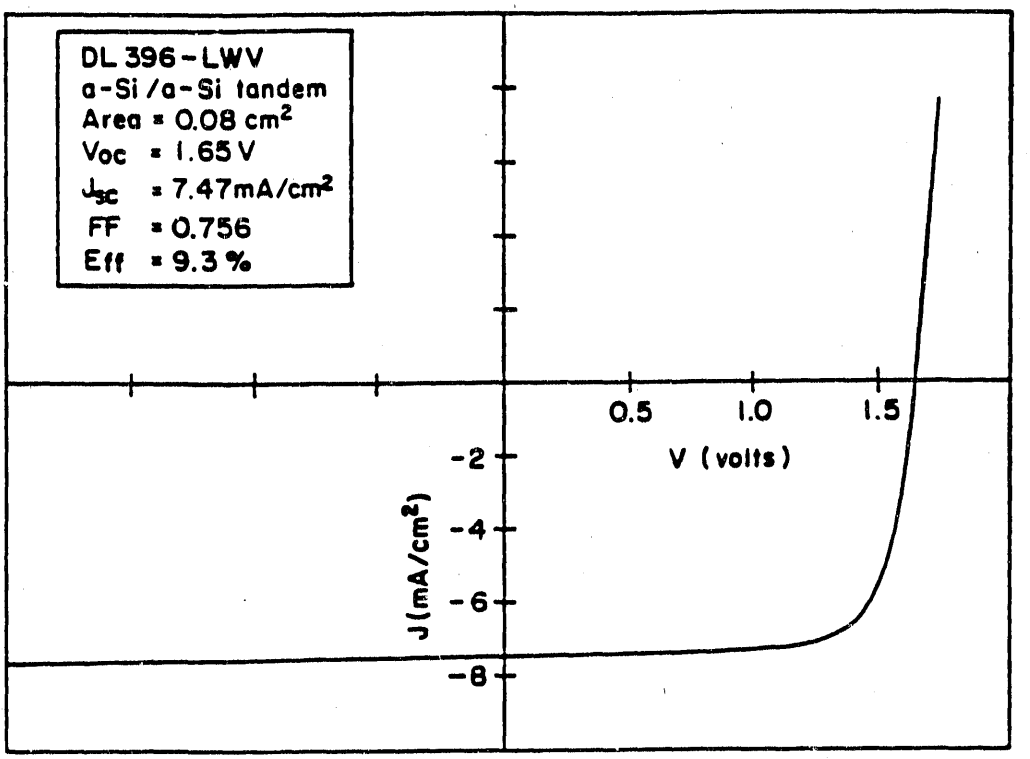

tandem cell using a back reflector, we have demonstrated an increase in bottom stack photocurrent of 8.5% through use of ZnO/Al as opposed to Al alone.

2.6 PHOTOSTABILITY

Years of observation and experience teach one that, while many cells light soak at about the same rate, it is nevertheless possible to observe considerable variety in light soak behavior - some cells are definitely more stable than most, and some cells degrade very rapidly [17, 18]. It is not always clear what factors are responsible for these differences, although certain factors are known to increase instability e.g. a thick ($>0.5\mu m$) i-layer, deposition from undiluted Si_2H_6, or deposition at low temperatures [17]. In the following sub-sections we examine the following questions:

a) does the use of a silicon carbide transitional i-layer impair photostability?

b) can the photostability of a cell be modified by any post-deposition treatment?

c) can photostability be influenced in any way by the nature of the contact materials (substrate or metallization)?

Many other studies relating to photostability have been conducted in the past, and are described in earlier subcontract reports e.g. [1, 8, 15, 17].

2.6.1 Effect of Silicon Carbide Transitional I-layer on Photostability

We have shown that the insertion of a silicon-carbide transitional i-layer between the p and i layers of a p-i-n device improves initial conversion efficiency by 6 - 18%. Typical gains in V_{oc} and J_{sc} are about 6% and 8%, respectively, with little change observed in FF. A natural question is whether the use of such a transitional i-layer has any effect on photostability.

A careful study was conducted to determine whether the use of a silicon-carbide transitional i-layer has any effect on single junction cell photostability. For this purpose, 8 runs were performed in the D1 system to prepare matched samples with and without a standard transitional i-layer. This layer (about 100 Å in thickness) was prepared using a $SiH_4/CH_4/H_2$ mixture in which the CH_4 flow was graded during deposition to vary the carbon content of the transitional i-layer. Two cells from each run were employed in the study to allow verification of consistency. For comparison purposes, cells from a good tandem junction run (with transitional i-layers) were also included in the study. Both dual ELH and HMI light sources were employed for J-V measurements. While the data differed slightly in detail, the overall conclusions drawn from both ELH and HMI data sets were identical. The cells were measured both before and after 188 hours broad-spectrum light soaking on load at 50°C. The study was then extended to 2590 hours of light soaking. The results (from the HMI data set) are shown in condensed form in Table V below.

Table V: Average efficiency of cells with and without a transitional i-layer (i_t) as a function of light soak time

Light soak* time (hours)	Efficiency (%) with i_t	Efficiency (%) without i_t	Junction type
0	8.44	7.12	single
188	6.24(-26.1%)	5.16(-27.5%)	
2590	4.97(-41.1%)	4.14(-41.9%)	
0	8.65	-	tandem
188	7.30(-15.6%)	-	

* on load, 50°C

It can be concluded that the presence of a SiC transitional i-layer (prepared according to our recipe) has no measurable effect on overall power loss, and that the initial gain in performance is retained. These results clearly indicate the desirability of incorporating a transitional i-layer into manufactured cells.

Distribution of light soak loss among photovoltaic parameters. A more detailed analysis of the data accumulated in the above study reveals that, while the overall percent power loss is the same for cells with and without a transitional i-layer, the relative changes in voltage, current, and fill factor are different, as shown in Table VI below.

Table VI: Percent change in single junction PV parameters upon light soaking*

Transitional i-layer	V_{oc}	J_{sc}	FF	Eff
Yes	-2.2%	-7.6%	-18.5%	-26.2%
No	+0.3%	-9.4%	-20.3%	-27.6%

*188 hours, maximum power point, 50°C

It can be seen that cells having a transitional i-layer lose 2.5% more in open-circuit voltage than cells without this layer, but that this is compensated by smaller drops in fill factor and short-circuit current, for a similar overall power loss.

2.6.2 Post-deposition Modification of Cell Stability

We have on occasion observed a "hardening" effect, wherein light soaked cells, after having been annealed to remove light-induced defects, exhibit increased resistance to subsequent light soaking. Later we learned that similar effects had been observed at Arco Solar [19].

Following the controversial report by Nevin et al.[20] we re-examined the hardening question using a high intensity pulsed xenon source (peak irradiation 2800 suns, pulse duration 6μs, 120 pulse/s) to light soak cells at 170°C, and followed this by 30 minutes annealing also at 170°C. These cells, and control cells which had been annealed but not soaked, were then light soaked at 1 sun, 50°C for 76 hours. We found that the cells which had been subjected to 100 s of intense irradiation degraded 31.7% compared to 35.2% for the control cells. The conclusion from this limited set of experiments is that the flash/anneal treatment can impart increased resistance to light soaking [1]. Further experiments are warranted in the general area of post-deposition modification of cell stability.

2.6.3 Influence of Contact Materials on Photostability

In this section we describe experiments designed to test whether the nature of the contact materials, i.e. front transparent conductor and back metallization, can affect the photostability of cell. Regarding the front contact material, we chose to compare tin oxide and tin oxide overcoated with zinc oxide, while for the back contact material we chose to compare aluminum and zinc oxide. For the front contact experiments, cells having the following structures were obtained from an inventory of existing devices:

$$SnO_2/p\text{-}i\text{-}n/ZnO/Al \quad \text{and} \quad SnO_2/ZnO/p\text{-}i\text{-}n/ZnO/Al$$

These cells had been deposited simultaneously on a 1 ft^2 SnO_2 - coated glass substrate (DL570RE) one half of which had been overcoated with ZnO prior to deposition of the amorphous silicon. The i-layer was 6000 Å in thickness. For the back contact experiments, existing unmetallized amorphous silicon was utilized (ET89-34-5, thickness 4200 Å), and back contacts of Al and ZnO/Al were applied. Thus, the structures of these devices were

$$SnO_2/p\text{-}i\text{-}n/Al \quad \text{and} \quad SnO_2/p\text{-}i\text{-}n/ZnO/Al.$$

Multiple cells in each category were then light soaked at open circuit, and measured using an HMI source. Very similar behavior was found for all cells in a given category.

Table VII summarizes the data concerning the influence of the front contact material.

Table VII: Comparison of the photostability of thick, single junction cells deposited simultaneously on SnO2 and SnO_2/ZnO.

Light soak* Time (Hours)	Efficiency (%) SnO_2	SnO_2/ZnO
0	8.79	8.29
620	5.05 (-42.5%)	5.97 (-28.0%)
1580	4.52 (-48.6%)	5.59 (-32.6%)

*Open circuit, 50°C.

Despite the lower starting efficiency of the cells on SnO_2/ZnO (an optical effect), these cells clearly soak more slowly than those on SnO_2, so that after 1580 hours soaking the cells on SnO_2/ZnO out perform those on SnO_2 by a considerable margin. The cells on SnO_2 experienced greater losses in both FF and J_{sc}. These experiments clearly demonstrate that the nature of the substrate can affect photostability.

Data concerning the possible influence of the back contact material is shown in Table VIII.

Table VIII. Comparison of the photostability of cells metallized with Al and ZnO/Al.

Light soak* Time (hours)	Efficiency (%) Al	ZnO/Al
0	7.97	8.34
1580	5.20 (-34.8%)	5.31 (-36.3%)

*Open circuit, 50°C

The light soak losses for cells metallized with Al and ZnO/Al are clearly very similar, but apparently slightly greater for the ZnO/Al contact (36.3% loss versus 34.8% loss). It is possible that this arises from a greater recombination rate in the i-layer resulting from improved light trapping with the ZnO/Al reflector.

Much work remains to be done in the area of photostability. Definitive studies must be conducted in the future in the following areas: effect of deposition temperature (in conjunction with substrate and p-layer effects), effect of i-layer gas flow rate, effect of boron level in the i-layer, effect of metallic impurities, effect of pre-deposition base pressure, and dependence of stabilized efficiency on panel temperature.

SECTION 3.0

NON-SEMICONDUCTOR MATERIALS

3.1 FRONT CONTACT MATERIALS

3.1.1 Tin Oxide

Our standard substrate for amorphous silicon deposition is soda lime glass coated with a transparent, conductive coating of tin oxide. Tin tetrachloride is used as the tin source, and a fluorinated hydrocarbon is used to dope the tin oxide with fluorine. A thin diffusion barrier of silicon dioxide is applied to the glass in order to block diffusion of sodium into the tin oxide during film growth, and to obtain better film coverage. The deposition of silicon dioxide from silane, oxygen and nitrogen, and the conductivity enhancement resulting from its use have been described earlier[15, 21]. Fluorine-doped tin oxide (with an SiO_2 diffusion barrier) is routinely produced in our laboratories with the following properties: sheet resistance 12 ohms/square, total transmission 80% (on glass), diffuse transmission 3%. At 8 ohms/square the diffuse transmission drops to 1%.

3.1.2 Tin Oxide Overcoated with Zinc Oxide

Because the tin oxide layer is formed at 500°C, and because tin oxide is a hard, generally inert material resistant to chemical attack, it is commonly assumed that its performance as a front transparent conductor in a p-i-n cell must be satisfactory. However, it is known that tin oxide is reduced by a hydrogen plasma, and to some extent by a silane plasma, while zinc oxide is not [22]. We therefore undertook to examine whether the properties of cells are altered in any way if the a-Si:H is deposited on zinc oxide. To accomplish this, we have employed standard SiO_2/SnO_2:F substrates overcoated with sputtered zinc oxide. The cell properties that we examined were initial photovoltaic performance, performance after light soaking (reported in section 2.6.3), and stability at elevated temperatures. One study in particular is described below.

Cells were prepared in run DL569 on a 1 ft^2 SiO_2/SnO_2 substrate, one half of which had been overcoated with ZnO. There was no O_2 plasma treatment of the substrate. The cells were metallized with Al, ZnO/Al or ZnO/Ag. Some samples were annealed one or more times in the range 150 - 170°C for 20 minutes. Table IX shows the average PV parameters obtained for the various combinations of front contact, back contact and annealing steps.

Table IX. Average PV parameters for p-i-n cells on SnO_2 and SnO_2/ZnO as a function of back contact type and number of anneals.

Structure	# Anneals	V_{oc}	J_{sc}	FF	Eff	R_s
SnO_2-pin-Al	0	821	15.6	69.0	8.5	4.6
SnO_2/ZnO-pin-Al	0	844	14.4	72.4	8.8	-
SnO_2-pin-ZnO/Al	1	821	15.1	69.1	8.6	4.6
SnO_2/ZnO-pin-ZnO/Al	1	848	16.1	71.7	9.8	4.6
SnO_2-pin-ZnO/Al	2	804	16.1	64.5	8.3	5.9
SnO_2/ZnO-pin-ZnO/Al	2	838	16.1	64.5	8.3	5.9
SnO_2-pin-ZnO/Ag	1	815	16.0	68.6	8.9	5.0
SnO_2/ZnO-pin-ZnO/Ag	1	847	15.6	71.7	9.5	4.8
SnO_2-pin-ZnO/Ag	3	814	16.5	67.0	9.0	5.0
SnO_2/ZnO-pin-ZnO/Ag	3	847	16.1	72.1	9.8	4.8

The following conclusions may be drawn:

a. The overcoating of SnO_2 with 500 Å ZnO increases V_{oc} by 20-30 mV (about 3%),decreases J_{sc} by 0.4-0.6 mA/cm^2 (about 3.3%), and in this study, it increased fill factor by about 5%.

b. It appears that overcoating with ZnO prevents FF loss during annealing. Thus, for all cells on SnO_2/ZnO, fill factors greater than 71% were maintained after annealing, while for cells on SnO_2 the fill factor dropped to 65-67% after two or three anneals.

The increase in initial fill factor seen here has so far not proven to be reproducible. Consequently, a reliable technique to improve initial efficiency through ZnO overcoating has not been realized. After extended light soaking, however, cells on SnO_2/ZnO appear to outperform cells on SnO_2, as described in section 2.6.3.

From spectral response data it was found that QE (400 nm) decreased from 0.58 to 0.52 upon overcoating the SnO_2 with ZnO. The overcoating also resulted in the appearance of interference fringes in the quantum efficiency plots. Observations concerning the effect of the back reflectors, although not pertinent to the overcoating study, were as follows. The current gain with ZnO/Al and ZnO/Ag, relative to Al, appear to be about 1 mA/cm^2 and 1-1.5 mA/cm^2, respectively. The figures for QE (760 nm) were 0.027 and 0.040, compared to 0.014 for Al.

3.2 SPUTTERED BACK CONTACT MATERIALS

Deposition of the back contact material, e.g. Al or ZnO, is preferably accomplished by sputtering rather than evaporation in order to improve step coverage at the laser-scribed interconnects, and to improve the thermal stability of the n-layer/Al contact. This section describes fundamental issues related to sputtering of the back contact, namely sputter-induced damage and contact stability, and the preparation and performance of ZnO-based back reflectors.

3.2.1 Sputter-induced Damage in p-i-n Devices

We have observed that sputtering of the back contact onto a-Si:H can cause two types of damage to p-i-n devices. The first type, believed to be due to high energy photons, appears to be unavoidable and causes degradation of the fill factor. It can, however, be rectified by annealing at 130°C for 20 minutes. The second type is manifested by visible breakdown of the silicon along dendritic paths. We believe an excessive flux onto the substrate of charged particles is responsible for this type of (irreparable) damage. The damage is increased by a) presence of a floating metal layer on top of the silicon e.g. sputtering Al onto glass/SnO_2/p-i-n/ZnO, and b) presence of isolated sheet metal close metal close to the substrate. It can be reduced by a) sputtering in an r.f. plasma,

b) proper orientation of the scribed films to ensure contact between the forming film and the underlying SnO_2), c) increase of the sputtering gas pressure, and d) use of improved magnetic field configurations to confine the charged species.

3.2.2 Back Contact Annealing Studies

A comparative study has been made of the behavior of cells metallized with evaporated Al and sputtered Al (2% Si) when subjected to successively increasing annealing temperatures. The results for fill factor are shown in Fig. 12. The ordinate, fill-factor deviation (%), is the average change in fill factor referred to the initial fill factor before annealing. Nine evaporated dots were studied, and 6 sputtered dots, all from run DL486. We conclude that a) cells metallized with sputtered Al must first be annealed to achieve optimal performance (by removal of sputter-induced damage), and b) cells with a sputtered Al (2% Si) back contact are more resistant to annealing at elevated temperatures. The latter result suggests that dissolution of Si in the Al has been suppressed through the use of Al (2% Si).

3.2.3 Preparation and Properties of Sputtered Zinc Oxide Films

A transparent, conducting film of zinc oxide appears to be a suitable material for both front and back contacts to a-Si:H p-i-n devices. We have produced zinc oxide thin films with good transmission (over 80% in the visible wavelengths) and good conductivity (2×10^3 ohm^{-1} cm^{-1}) by R. F. magnetron sputtering from a compound target doped with alumina. In this way, zinc oxide films with sheet resistances less than 10 ohms/sq. were prepared with visible transmission higher than that of similar sheet resistance tin oxide. This is shown in Fig. 13. More detailed optoelectronic and structural properties of ZnO:Al were described in previous reports [1, 15, 16].

Our previously reported Auger analysis of the films was based on calibration samples prepared at another institution. This procedure casts doubt on the quantitative information obtained. In order to obtain a reliable measure of the stoichiometry, RBS analysis was carried out on samples prepared by sputtering, and the results were used to calibrate subsequent Auger measurements. The RBS analysis was performed by Evans East, Inc. and yielded the following areal density:

O: 5.23×10^{17} atoms/cm^2

Zn: 4.71×10^{17} atoms/cm^2

The stoichiometry is therefore $Zn_{1.0}O_{1.1}$. Low levels of Ar and Al were also detected.

Figure 12. Percent change in fill factor (referred to initial fill factor) versus anneal temperature for cells with evaporated Al back contacts and sputtered Al (2% Si) back contacts when subjected to 20 minute periods of annealing at successively higher temperatures.

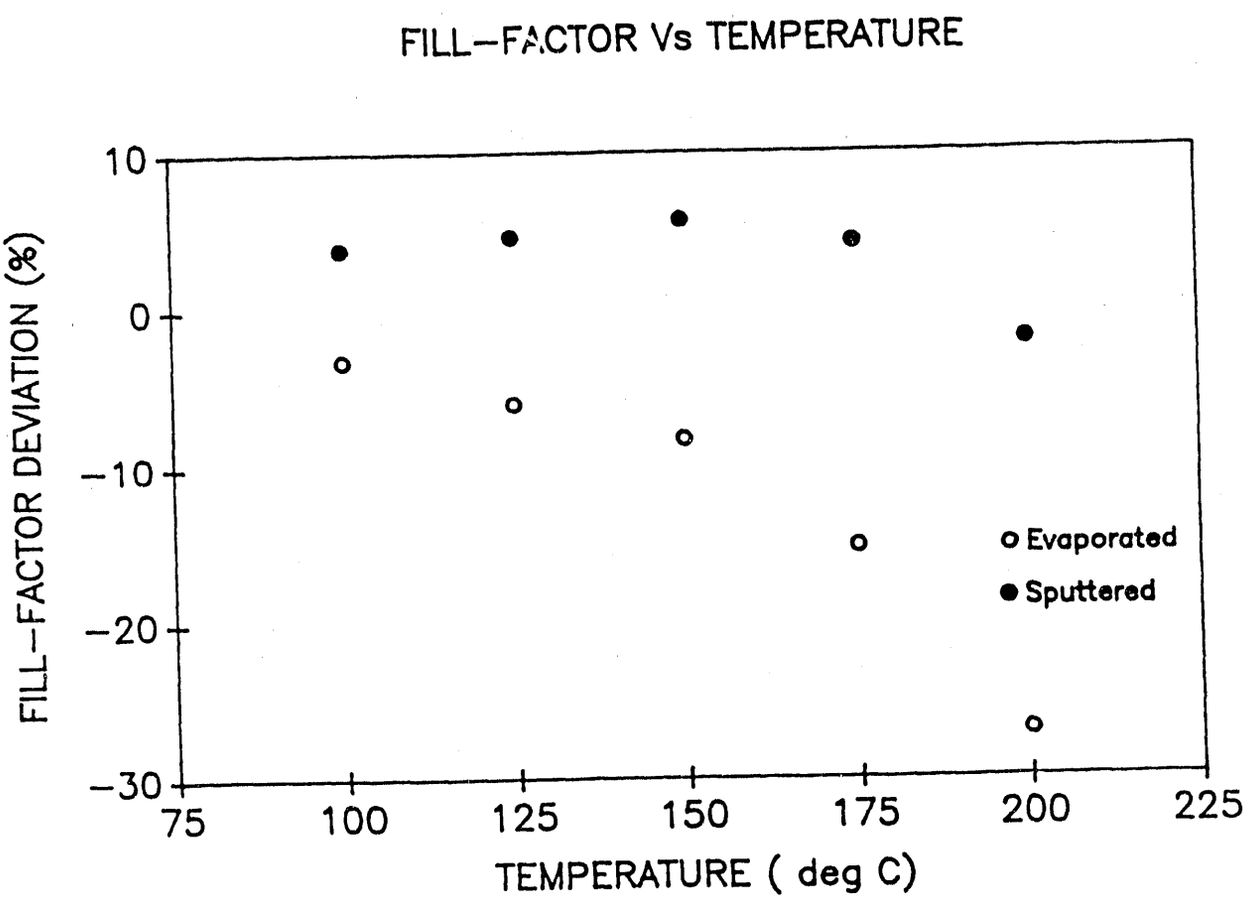

Figure 13. Transmission spectrum of 9.5 Ω/□ ZnO:Al (sputtered) compared with that of 10.5 Ω/□ SnO_2:F (APCVD)

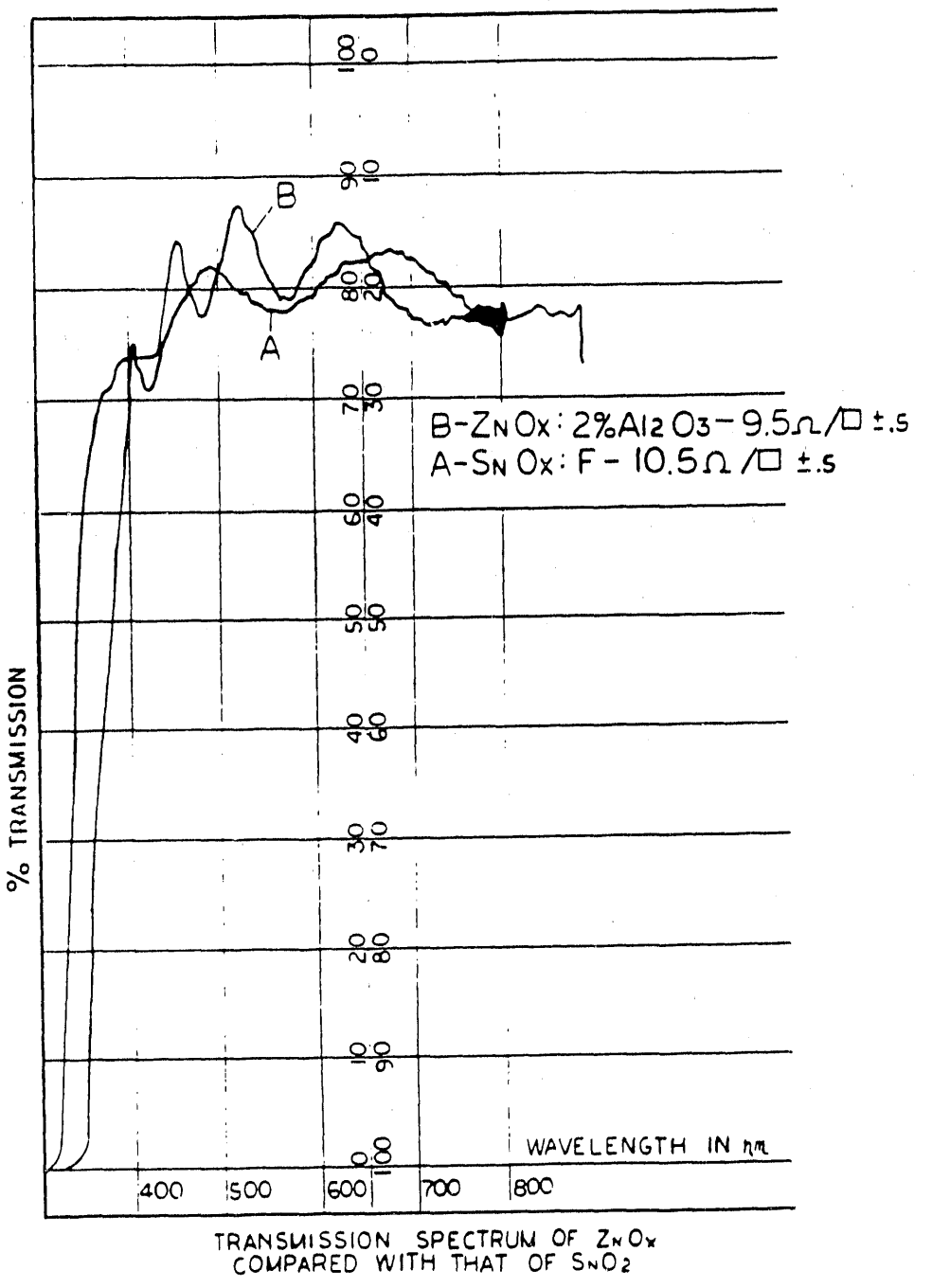

TRANSMISSION SPECTRUM OF ZnO_x COMPARED WITH THAT OF SnO_2

Annealing studies of the films have been performed. Table X shows the dependence of sheet resistance upon annealing time for 800A films of sputtered ZnO:Al annealed at 150°C in both air and argon atmospheres. The film annealed in air showed a 23% increase in sheet resistance after 150 hours annealing. The increase is attributed to removal of oxygen vacancies, which are known to supply carriers in many metallic oxides. The much smaller increase in the case of annealing in argon could be due to the smaller removal of such defects by interstitial oxygen.

Table X. Dependence of sheet resistance upon time of annealing at 150°C for 800Å ZnO:Al films annealed in air and argon.

Annealing time (hours)	Sheet resistance (Ω/□) Argon ambient	Air ambient
1	88.9	92.0
3	88.5	92.5
28	88.7	98.0
48	88.7	103.5
55	89.8	106.0
150	91.5	113.0

Over time the zinc oxide sputtering target changed color and decreased in surface resistivity. This suggests that the target was becoming progressively metal rich. Consistent with this, zinc has a higher sputtering yield than oxygen for the same ion energy. The zinc-rich surface layer produces zinc-rich films with poor transmission. A possible solution is a periodic scrubbing of the surface layers with an abrasive material to expose the desired composition of the underlying layers.

3.2.4 Zinc Oxide Based Back Reflectors

Highly reflective back contacts based on zinc oxide have been incorporated as a standard processing step in both small area devices and modules. The previously noted problem of reduced fill factors was rectified by annealing the devices following sputter deposition of the zinc oxide. As noted in sections 3.2.1 and 3.2.2, the annealing removes sputter-induced damage to the amorphous silicon. To compare the merits of various back reflector schemes, substrates were cut from a single silicon run (94-39-9) and metallized with Ag(evap), Al-2% Si (sputt), ZnO (sputt)/Al, ZnO (sputt)/Cu, and ZnO (sputt)/Ag. The performance of these devices (J_{sc} and FF) is shown in Table XI as a function of successive annealing treatments. In this study ZnO/Ag yielded the highest short-circuit current and was found to be stable. However, the initial yield of good cells for ZnO/Ag and ZnO/Cu was only half that for ZnO/Al.

Table XI: Performance of cells metallized with various back reflectors and subjected to successive annealings.

Metallization	J_{sc}(mA/cm^2)/FF(%) after successive indicated treatment					
	Initial	130C/20m	130C/20m	150C/20m	150C/20m	170C/35m
Ag(evap)	13.2/68.0	14.1/63.7	15.4/66.2	14.9/66.7	14.9/66.3	-
Al(sputt)	13.6/66.2	13.7/69.3	13.7/69.0	13.8/70.0	-	13.6/69.7
ZnO(sputt) /Al	15.0/65.6	15.0/68.0	15.1/68.2	15.2/68.8	-	15.1/68.4
ZnO(sputt) /Cu	15.4/65.4	15.5/67.7	15.6/67.2	15.5/67.6	-	15.2/65.8
ZnO(sputt) /Ag	16.1/65.8	16.0/67.7	16.2/67.7	16.1/69.0	-	16.1/68.9

We have also studied the performance of ZnO/Al reflectors as a function of ZnO thickness in order to determine the optimal ZnO thickness. Again, substrates were cut from a single silicon run (89-34-5) and were metallized with various thicknesses of ZnO followed by Al. Table XII shows the effect of these reflectors on short-circuit current density and quantum efficiency at 700 nm. Optimum performance was obtained for 800 Å ZnO.

Table XII: Effect of back reflectors of the form ZnO/Al on short-circuit current density and quantum efficiency at 700 nm as a function of ZnO thickness.

ZnO thickness (A)	ΔJ_{sc} (%)	$r_2 = \frac{QE[700\ nm]}{QE[peak]}$	r_2/r_1,*
100	1.9	0.201	1.12
200	4.9	0.241	1.34
400	5.4	0.272	1.51
800	7.7	0.324	1.71
6400	4.1	0.280	1.56

*r_1 = QE(700 nm)/QE(peak) for control cells without ZnO (0.18-0.19)

Other studies have shown that, as far as improved red response and J_{sc} are concerned, ZnO/Cu is slightly superior to ZnO/Al, and ZnO/Ag is considerably superior. A number of 1 cm^2 cells were fabricated with efficiencies over 10% with ZnO/Ag as the back reflector (see section 2.4). The performance gain due to the presence of a ZnO back reflector is thought to depend on factors such as the granularity of the front TCO, the thickness of the i-layer, and the reflectivity of the back electrode. The reflectivity of the metal electrode depends not only on the type of metal, but also on its texture, and on reactions that occur when an interface is formed with the underlying material, or when the structure is annealed [23]. These effects have not yet been separated, and may account for some variability seen in the overall performance gain. In general, however, current gains of 7.5% with ZnO/Al, and 11% with ZnO/Ag can be relied upon.

Techniques other than R.F. sputtering of ZnO from a compound target are probably capable of higher deposition rates, and would be desirable in a large scale production environment. Candidate techniques are D.C. reactive sputtering, LPCVD and APCVD. The deposition of ZnO back reflectors by APCVD was attempted in collaboration with Professor R. Gordon's group at Harvard University. Device structures on which ZnO was deposited by APCVD at 180°C showed considerably higher series resistances than did control cells. This was attributed to poor doping efficiency of the ZnO at this temperature and oxidation of the a-Si:H surface due to the oxygen rich and reactive atmosphere of the APCVD furnace.

SECTION 4.0

SUBMODULE RESEARCH

4.1 APPROACH TO SUBMODULE FABRICATION

Our R&D submodules consist of 1 x 1 ft^2 (929 cm^2) glass substrates on which the solar cell is deposited. The solar cell structure may take one of the many forms described under Subtask B1. On the glass, 30 cells, each measuring nominally 1-cm x 30-cm are series connected. Patterning is accomplished by laser scribing. Occasionally, R&D makes use of 1 ft x 3 ft and 5 ft x 2.5 ft submodules that are produced in factory equipment.

The following major steps constitute the submodule fabrication process. First, the front transparent conductive oxide (TCO) is placed on glass measuring nominally 5 ft x 2.5 ft. The glass is then cut into square foot pieces, and the TCO is laser patterned. Semiconductor material is deposited onto the TCO. At this point, there is an option to either laser scribe the semiconductor material or place a back contact on the semiconductor material and then laser pattern the resulting combination. In any event, onto the developing cell is deposited a final back contact, which makes electrical contact to the front TCO through the laser scribe in the semiconductor. The back contact is then laser patterned. If suitable, the submodule is encapsulated.

4.2 POWER LOSSES IN SUBMODULES

4.2.1 Front TCO Sheet Resistance

For R&D submodules, the front textured TCO is most often a bilayer consisting of fluorine doped tin oxide and a sublayer of silicon dioxide. Both layers are deposited by our own APCVD process. We also make use of sputtered zinc oxide, placed as an overcoat on the tin oxide.

Sheet resistance of this front TCO contact is around 10 ohms per square. From a computer program based on collection length theory and developed at Chronar, we can calculate the power loss due to such sheet resistance. Input for this calculation are intrinsic photovoltaic parameters (Voc, Jsc, FF) measured on small area cells isolated from the submodule. Thus, for typically achieved Voc around 0.85 V, Jsc around 15.6 mA/cm^2, and intrinsic FF around 70 %, we calculate that a front TCO sheet resistance of 10 ohms/square drops submodule power output by about 5 %.

Tin oxide deposition is being improved, and textured layers with high transmission and

reduced sheet resistance should be available in the not too distant future.

4.2.2 Contact Resistance in Interconnection

There are several ways in which poor electrical contact can occur between the back contact of one cell and the front TCO contact of an adjacent cell. Step coverage sometimes occurs when the back metal contact is evaporated using point, or even line sources. Occasionally, because of peculiarities in p-layer constitution, laser scribing of the silicon fails to remove all resistive material from the front TCO. In general, however, using sputtered back metal contacts, contact resistance due to interconnection can be kept significantly below 0.3 ohm-cm, where the unit of length is measured along the scribed connection. Using the computer program as mentioned above, such contact resistance amounts to about 0.5 % loss of total panel power.

4.2.3 Shunts

4.2.3.1 Shunt Quality

A method was developed for estimating the power loss in a-Si submodules due to shunting defects, no matter what their origin. A particular convenience of this method lies in the fact that only cell-to-cell dark isolation resistances need be measured. Thus, I-V measurements on irradiated submodules need not be made.
In this method, we first write the power output of a panel, P, as follows.

$$P=\sum \frac{P_{si}}{P_{ui}} P_{ui}$$

where P_{si} is the power of the i^{th} (shunted) cell, P_{ui} is the power of the i^{th} cell if it were unshunted, and the summation is to occur over all N cells of the panel. We then define shunt quality, Q_s, as the ratio of the actual (shunted) panel power to the unshunted panel power:

$$Q_s=\frac{P}{NP_{ui}}=\frac{1}{N}\sum \frac{P_{si}}{P_{ui}}$$

where we have assumed that the unshunted, ideal panel is uniform (P_{ui} = constant).

For a real panel, the ratio P_{si}/P_{ui} can be determined experimentally by measuring the cell output with shunts imposed across the cell. Fig. 14 contains such data and

Figure 14. Measured percent power of a 1 cm x 30 cm cell as a function of shunt resistance

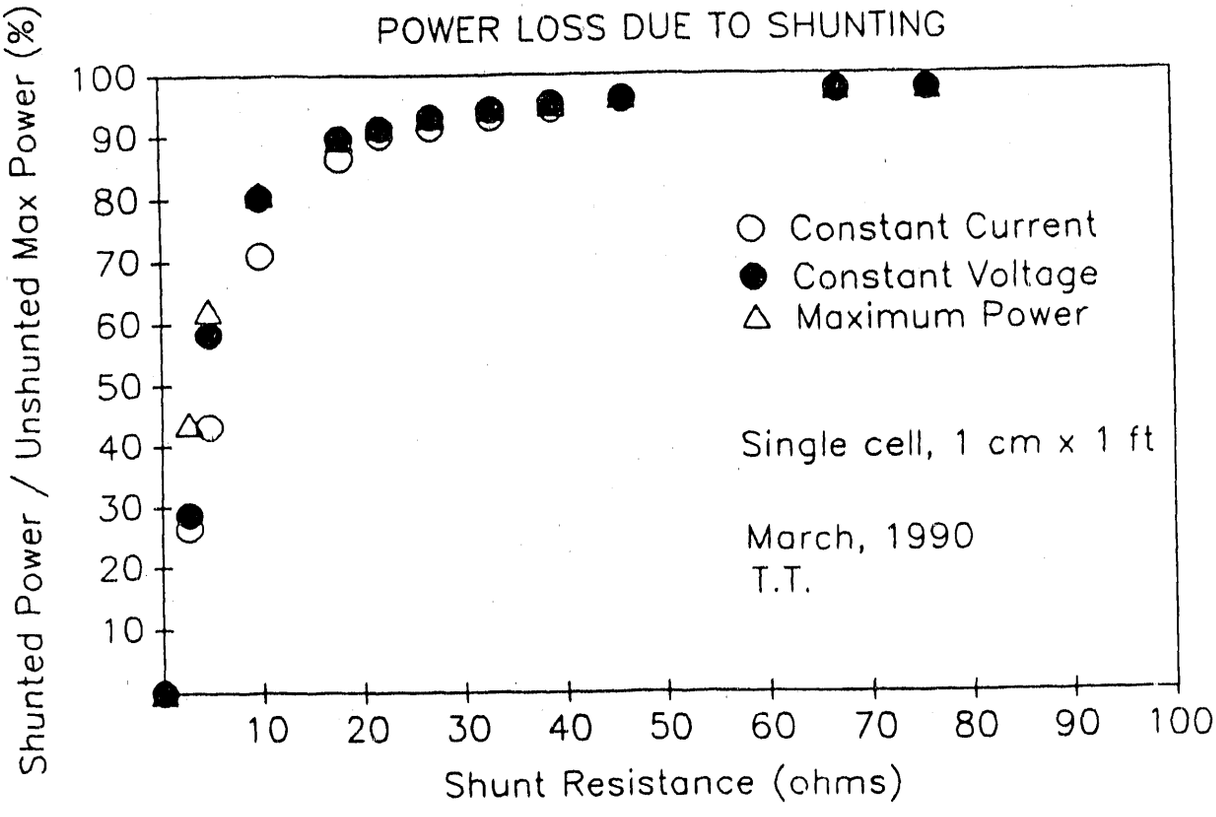

consists of three correlations. The maximum power correlation is obtained by recording the power output of the cell at the maximum power point, which shifts with different shunt values. The constant current curve is obtained by measuring the power output of the cell at the maximum power point current of the unshunted cell. The constant voltage curve is obtained by measuring the output of the cell at the maximum power voltage of the unshunted cell. If only a small amount of shunting occurs in the panel, then one should choose the constant current correlation, for then, the shunted cell will be forced to pass a current very near the maximum power current of the rest of the panel. Practically speaking however, the three correlations do not differ widely.

Curves such as that provided by Fig. 14 could also be calculated theoretically using the collection length model.

Results of this method provide reasonably accurate estimates of shunting power loss, as shown in Fig. 15. For this figure, many combinations of shunts were placed across 24 series connected foot-long cells. The string output was measured under one-sun illumination and plotted against Q_s, as calculated from Eq. 2, using the constant current correlation.

It is expected that this method would also give good results for cells longer than one foot, providing the resistance of the back metal contact remains much smaller than the shunts of interest.

4.2.3.2 Types of Shunts

We refer the reader to previous reports under this contract for detailed descriptions on the several types of shunting defects that have been identified. We also refer the reader to those reports for descriptions of the various techniques developed to remove shunting defects, most notably heat treatment, current blasting and electrochemical etching.

4.2.3.3 Shunting Power Loss

Because of relatively pinhole free silicon deposition and the effectiveness of the laser/etch technique of back contact patterning (explained below), shunting losses in our best submodules are small. Shunting power losses below 2 % can be routinely obtained for square foot submodules. Nevertheless, it has been reported that planar shunting, if initially less than about 5000 ohm cm^2, can decrease by a factor of 4 - 12 upon light soaking, and lead to power losses over and above what is attributable to the Staebler-Wronski effect [24]. Since the likelihood of shunting is greater for thin i-layers, this effect can move the i-layer thickness for maximum stabilized efficiency in the direction of thicker i-layers.

Figure 15. Correlation between actual module percent power and that calculated from shunt quality, Q_s

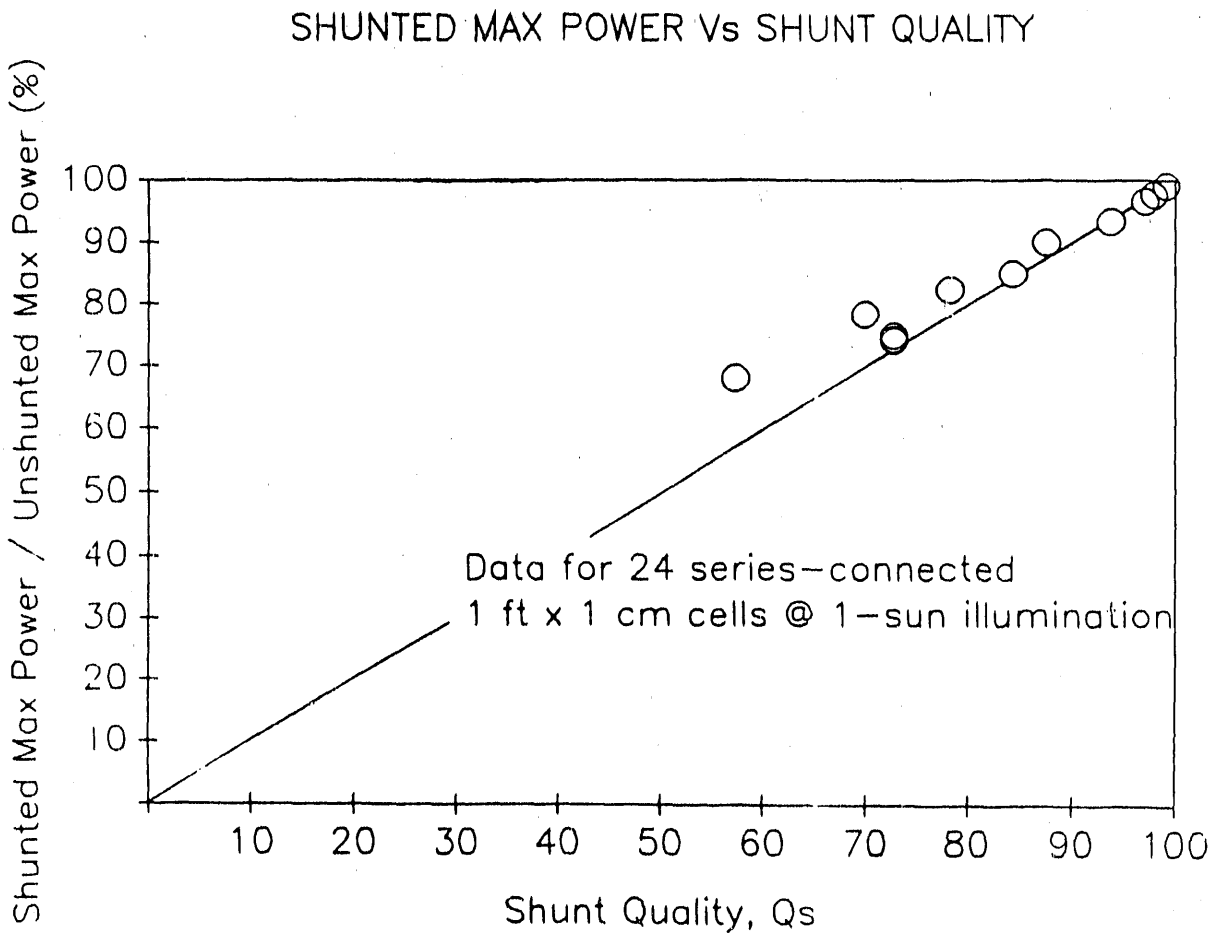

4.2.4 Patterning Losses

As explained in the next section, active area loss due to cell patterning in current R&D panels can be routinely limited to about 3 % of total active area.

4.2.5 Nonuniform Deposition and Mismatching

When nonuniformities in film depositions produce areas of the submodule having differing photovoltaic parameters (Jsc, Voc, FF), the submodule assembly prevents each area from performing at its independent maximum power point. This "detuning" of operation is similar to the mismatching that occurs among modules when placed in arrays and constitutes a significant sources of power loss within submodules.

We estimate that, in our best submodules (with silicon from the D1 System), as-deposited power loss due to mismatching amounts to a few percent of total power output. Upon light soaking, however, since Staebler-Wronski degradation of cells tends to lessen initial variations in photovoltaic parameters, losses due to mismatching are believed to be reduced. In fact, the change of mismatch behavior may explain at least in part why the often observed stability of large submodules is greater than that of small area cells.

In order to investigate quantitatively the degree to which current mismatch in series connected cells could reduce submodule performance, we obtained data on a submodule with a single cell shaded so that its Jsc was 20 % of its unshaded amount. The unshaded submodule output was 3.5 W, at a maximum power point voltage (Vm) of 15.5 V. The individual Vm for each unshaded cell averaged 0.49 V, with corresponding average Voc 0.71 V. With the shaded cell, and with the submodule biased at its unshaded Vm of 15.5 V, the panel output dropped to 1.39 W (47 % of the unshaded value). The shaded power point shifted, yielding a corresponding Vm of 9.83 V, and maximum power output of 1.85 W (47 % of the unshaded value). With the submodule biased at the unshaded Vm of 15.5 V, the shaded cell was driven to - 3.3 V (reverse bias), a value that most cells with reasonably good fill factor could withstand. In addition, with the 15.5 V submodule bias, the individual unshaded cells were operating around 0.69 V, quite removed from their individual Vm of 0.49 V, and quite close to their individual Voc of 0.71 V.

Thus, with only one current limiting cell that doesn't break down under significant reverse bias, serious detuning of operation occurs within a panel as a whole. For maximum efficiency, then, silicon i-layer thickness uniformity should be strictly maintained for all cells, and in particular, for cells near the edge of the panel, where, because of typical deposition chamber designs, silicon thickness can drop to less than half the silicon thickness present in the bulk of the panel.

Parallel cell connections impose the same voltage drop across the cells. In particular, when different areas of a photovoltaic panel having different power point voltage outputs

are connected in parallel by means of metallization in the form of a single cell, there is a net loss of potential power output because of the detuning that occurs among different areas of the cell. Thus, for maximum panel efficiency, p-layer performance should be strictly maintained throughout the panel.

A detailed analysis of power losses in one of the D1 system submodules resulted in an estimate of mismatch losses as follows. The submodule investigated has the structure Glass/SiO_2/SnO_2/pin/ZnO/Al and measured as follows:

Voc	Isc	FF	Pm	Ap Area	Ap A Eff
25.4 V	414 mA	61.4 %	6.46 W	868 cm^2	7.44 %

Small area cells, both 1-cm^2 and 0.08 cm^2 sizes, were isolated on this submodule in six positions across the submodule. The smallest cells provided fill factor and Voc data, while the 1-cm^2 cells provided Jsc data. From this data, a spatially averaged small area cell efficiency for the panel was calculated to be 8.7 %. The interconnected panel thus measured approximately (8.7 - 7.4)/8.7 = 15 % lower than this intrinsic small area efficiency.

Detailed measurements on sheet resistance, contact resistance and isolation resistance gave the following results for power loss: 5 % due to tin oxide sheet resistance; 1 % due to contact resistance in the interconnection, 0.6 % due to all kinds of shunting, and 4.6 % due to loss of active area. Total accountable losses thus amount to 5 + 1 + 0.6 + 4.6 = 11.2 %, leaving 15 - 11 = 4 % unaccountable, and presumably due to mismatching.

Considering all our depositions, our best small area cells with the same structure as in this submodule are around 10 %. Since the submodule analyzed above is among our highest in efficiency, nonuniformities and mismatch losses can be seen to significantly limit output in our large area interconnected panels.

Our capability of depositing uniform silicon layers over square foot areas has been greatly improved with the Eureka System and the recent operational status of the D2 System. Unfortunately, insufficient optimization of these systems in the contract period has limited progress in transferring our best small area results to the submodule level.

4.3 LASER PATTERNING

4.3.1 2-Step (Fused Interconnection)

Exploratory experiments were conducted in order to evaluate methods of laser scribing that, in one process step, would provide both isolation of the back contact and interconnection between the back contact and front TCO (fused interconnection). For the fused interconnection, experiments were conducted passing laser beams of wavelengths 0.53

and 1.06 μm both through the glass side and through the back side of the cell. Back contacts of aluminum and of aluminum overcoated with various materials were included in the study. Progress was obtained in achieving contacts with contact resistances around 1 ohm-cm (sufficient to keep contact losses below 2 % of total panel output), and some of these contacts showed stability under annealing for over a month at 100 °C.

The project was however discontinued since the value of the process to Chronar was deemed not worth the effort, particularly since acceptable progress was made on the standard 3-step method in conjunction with computerized tracking (described below).

4.3.2 3-Step Laser Scribing with Computerized Tracking

Our current laser scribing capability at Chronar routinely allows a 3 % loss of active area because of the interconnection. This relatively low loss is achieved with a 50 μm wide scribe in the front TCO, 100 μm wide scribes in both the silicon and silicon/back contact, and two 25μm gaps between the scribes. The sum of these widths is 300 μm, or 3 % of a cell spacing of 1 cm.

The front TCO scribe, being the scribe first performed, serves as the reference for the computerized tracking that controls the subsequent two scribes.

Further improvements on this scribing process would involve the purchase of optics with higher resolution, in order to halve the dead space between scribes, and of lasers with improved stability, in order to halve the width of the three scribes. (The current laser x-y tables would not require upgrading, having already a resolution of 1.25 μm.) Thus, with an upgrade in equipment, the existing process can maintain below 2 % lost area due to the three scribe interconnection.

4.3.3 Laser/Etch Technique for Back Contacts

Because of the variety of back contacts experimented with in research, and because of the sensitivity laser scribing exhibits with respect to the material being scribed, we found it necessary to use a laser/etch technique in patterning the back contact. Such a technique insures excellent cell isolation with a variety of cell structures.

With this technique, a mask is first sprayed onto the back of the cell. The laser scribing is then executed, patterning the mask along with the back contact. At this point, cell isolation is usually poor, since the lasering operation is often not optimized. Thus, the final step is to submerge the scribed area in a chemical etchant that subsequently removes shunting particles within the scribes.
Initially, we found photoresist a suitable masking material, however, a commercially available spray based on cellulose was found to be more convenient. The cellulose spray can be applied easier, and it has the advantageous property that, once being exposed to etchant, it washes away with plain water.

With the laser/etch technique applied to a vast variety of back contacts, we routinely achieve cell-to-cell isolation featuring negligible power loss due to scribe related shunting.

4.3.4 Annealing and Laser Performance

Annealing was found to be a convenient way to restrict peeling of certain back contacts during laser scribing. In particular, when zinc oxide is used as a back reflector, onto which aluminum or silver is placed for enhanced reflection and electrical conduction, an annealing step prior to lasering prevents the severe peeling that would otherwise occur. Generally, a 20 - 60 minute anneal at 150 - 160 °C is sufficient.

4.4 BEST MODULE PERFORMANCE

4.4.1 Single Junction

The following data was obtained by SERI's measurement of Chronar's highest efficiency square foot single junction submodule, which has the structure: Glass/SiO_2/SnO_2/pin/ZnO/Al.

Voc	Isc	FF	Pm	Ap Area	Ap A Eff
24.2 V	404 mA	67.0 %	6.59 W	873 cm^2	7.55 %

The I-V curve for this submodule is shown in Fig. 16.

Many important advances established within this research subcontract (e.g. use of a silicon dioxide barrier layer on soda lime glass, carbon-graded p and i_t layers, laser isolation of the back contact) have been applied within the Eureka project, and have allowed the fabrication of a 1.2 m^2 module having a power output of 74.4 W, a world record for a monolithic thin film module [25]. The I-V curve for this module is shown in Fig. 17.

Figure 16. I-V curve for a 1 ft^2 single junction module with ZnO/Al reflector (aperture area efficiency 7.55%)

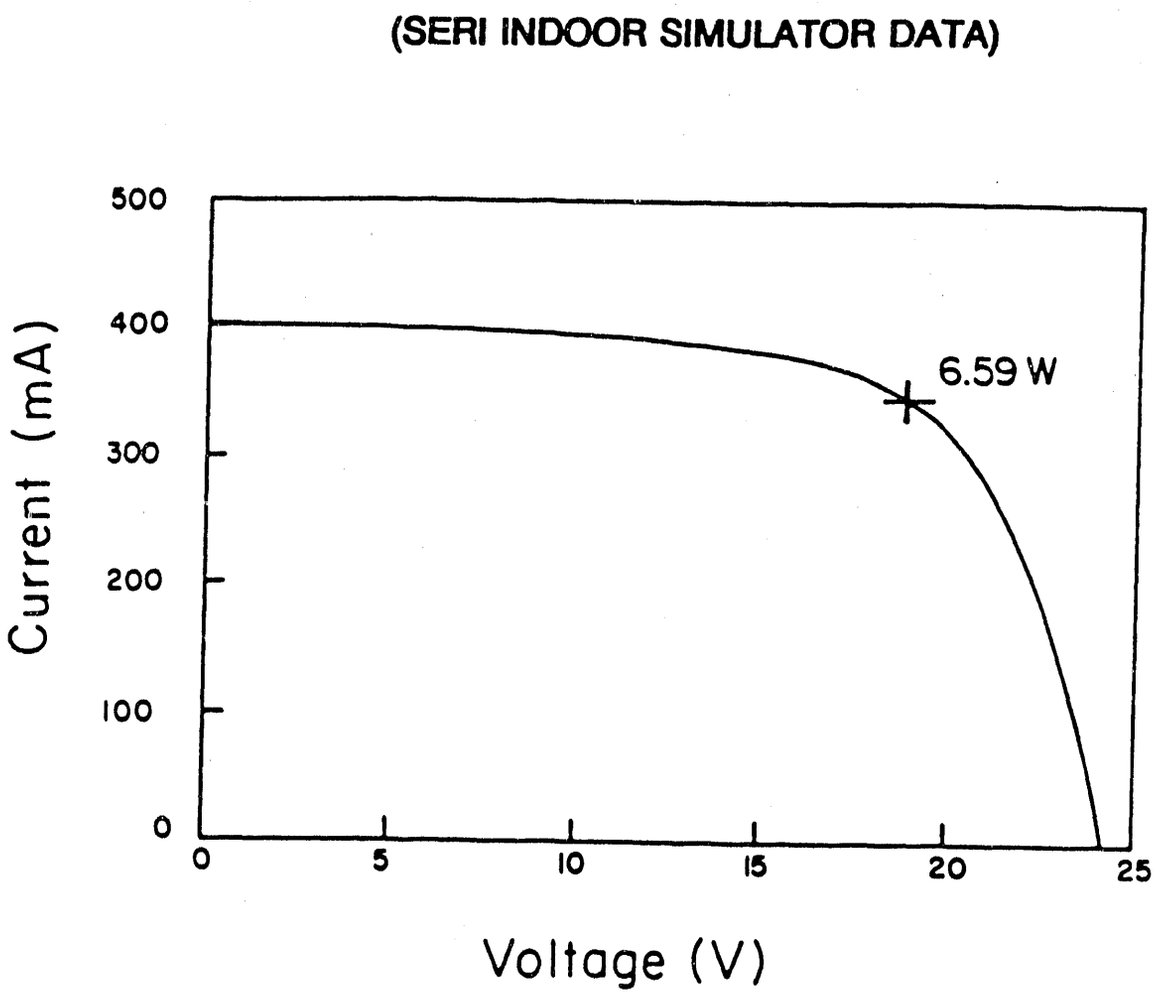

Intensity	= 100 mW/cm^2	FF	= 0.67
Temp	= 25° C	Pm	= 6.59 W
Voc	= 24.2 V	Aperture area	= 873 cm^2
Isc	= 404 mA	Ap. area efficiency	= 7.55 %

Figure 17. Outdoor measurements on a 1.2 m^2 Eureka module; power output 74.4 W, a world record for a monolithic thin film module. (Data acquired on April 6, 1990 at the SERI PVF module testing and performance facility).

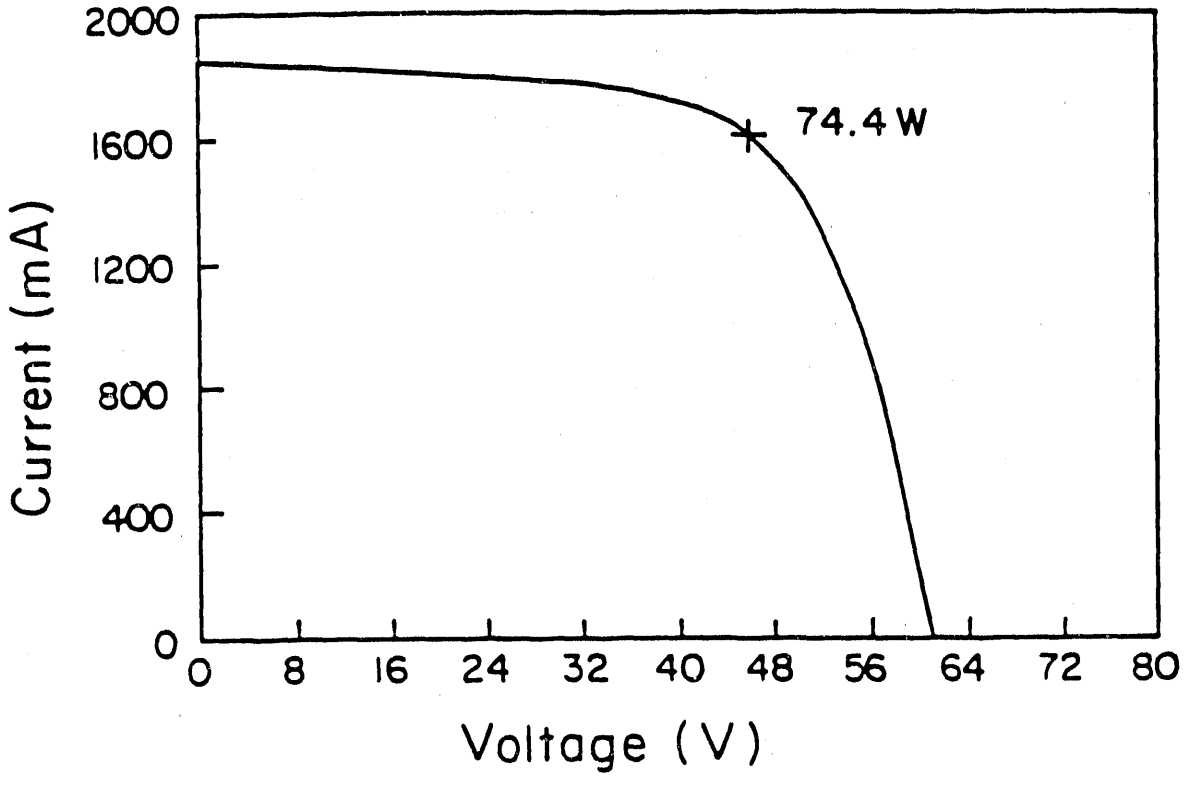

Insolation = 1004 W/m^2	**Vm = 46.4 V**
Temp = 32.6°C	**Im = 1602 mA**
V_{oc} = 61.0 V	**Pm = 74.4 W**
I_{sc} = 1848 mA	**Aperture area = 11,900 cm^2**
FF = 66.0%	**Ap. area efficiency = 6.23%**

4.4.2 Tandem Junction

The following data was obtained by Chronar's measurement of its highest efficiency tandem junction square foot submodule, which has the structure, Glass/SnO_2/pin/pin/Al:

Voc	Isc	FF	Pm	Ap Area	Ap A Eff
48.3 V	189 mA	66.1 %	6.04 W	842 cm^2	7.17 %

The following data was obtained by SERI's measurement of Chronar's highest efficiency tandem junction 1 ft x 3 ft submodule, which has the structure: Glass/SiO_2/SnO_2/pin/pin/Al:

Voc	Isc	FF	Pm	Ap Area	Ap A Eff
46.7 V	548 mA	64.1 %	16.4 W	2,555 cm^2	6.42 %

REFERENCES

1. A.E. Delahoy, F.B. Ellis, Jr., C. Kothandaraman, H. Shade, T. Tonon, and H. Weakliem, Semi-Annual Subcontract Report 16 March 1989-30 November 1989, Subcontract No. ZB-7-06003-1 (SERI/TP-211-3667. Available NTIS: Order No. DE9000-0320).

2. A.E. Delahoy, F.B.Ellis, Jr, E. Eser, S.C. Gau, H. Volltrauer, and Z. Kiss, "Single Chamber Amorphous Silicon Manufacturing Process, "6th European Photovoltaic Solar Conference, London, April 1985. D. Reidel Pub. Co. pp. 670-676.

3. S.C. Gau, H. Volltrauer, F. Faras, A.E. Delahoy, E. Eser, and Z. Kiss, "Manufacturing Process for Interconnected Submodules of Hydrogenated Amorphous Silicon Photovoltaic Panels," Appl. Phys. Lett. 48(12), 1317-1319 (1985).

4. M. Bohm, A.E. Delahoy, F.B. Ellis, Jr., E. Eser, S.C. Gau, F.J. Kampas, Z. Kiss, K.R. Ramaprasad, H. Volltrauer, and H.A. Weakliem, "Single Chamber Manufacturing Process for Amorphous Silicon Solar Cells," Proc. 18th IEEE Photovoltaic Specialists Conference, (IEEE, NY 1985) pp. 888-893.

5. I. Balberg, A.E. Delahoy, and H.A. Weakliem, "Self-Consistency and Self-Sufficiency of the Photocarrier Grating Technique." Appl. Phys. Lett. 53, 992 (1988).

6. R.S. Crandall, K. Sadlon, J. Kalina, and A.E. Delahoy, "Direct Measurement of the Mobility-Lifetime Product of Holes and Electrons in an Amorphous Silicon p-i-n Cell." Mat. Res. Soc. Proc. Vol. 1989, pp. 423-427.

7. I. Balberg, A.E. Delahoy, and H.A. Weakliem, "Light Intensity Dependence of the Ambipolar Diffusion Length in Hydrogenated Amorphous Silicon," Proc. 20th IEEE Photovoltaic Specialists Conference, (IEEE, NY, 1988). pp. 352-356.

8. A.E. Delahoy, and F.J. Kampas, Semi-annual Subcontract Report 16 March 1988 - 15 September 1988, Subcontract No. ZB-7-06003-1 (SERI/STR-211-3528. Available NTIS: Order No. DE89009439).

9. A.E. Delahoy, E. Eser, and F.J. Kampas, Annual Subcontract Report 16 March 1987 - 15 March 1988, Subcontract No. ZB-7-06003-1 (SERI/STR-211-3487. Available NTIS: Order No. DE89000886).

10. S. Nakano, S. Okamoto, T. Takahama, M. Nishikuni, K. Ninomiya, N. Nakamura, S. Tsuda, M. Ohnishi, Y. Kishi, and Y. Kuwano "High Absorption-Coefficient and Stable a-Si for High Efficiency Solar Cells" Proc.21st. IEEE Photovoltaic Specialists Conference (IEEE, NY 1990) pp. 1656-1661.

11. F.B. Ellis, Jr., and A.E. Delahoy, "Chemical Vapor Deposition of Boron-doped Hydrogenated Amorphous Silicon" Appl. Phys. Lett 47 (2), 135 (1985).

12. H. Tarui, T. Matsuyama, S.Okamoto, Y. Hishikawa, H. Dohjo, N. Nakamura, S. Tsuda, S. Nakano, M. Ohnishi, and Y. Kuwano "Preparation and Properties of High Quality p-type a-SiC Materials for a-Si Solar Cells" Technical Digest of the International PVSEC-3, Tokyo, Japan, 1987.

13. W. Zongyan, A. Lloret, J. -M. Siefert, P. Roca Cabarrocas, B. Equer in Amorphous Silicon Technology (Mater. Res. Soc. Proc. Vol. 149, MRS Pittsburgh, 1989) pp. 291-296.

14 A. Catalano et al., Final Subcontract Report, 1 February 1989 - 28 February 1990, Subcontract No. ZB-7-06003-2 (SERI/TP-211-3906. Available NTIS: order No DE90000356).

15. A. E. Delahoy, F. B. Ellis, Jr., F. J. Kampas, T. Tonon, and H. A. Weakliem, Annual Subcontract Report, 16 March, 1988 - 15 March 1989, Subcontract No ZB-7-06003-1 (SERI/STR-211-3609. Available NTIS: Order No. DE89009515).

16. A. E. Delahoy, "Recent Developments in Amorphous Silicon Photovoltaic Research and Manufacturing at Chronar Corporation." Solar Cells, 27 (1989) 39-57.

17. A. E. Delahoy, E. Eser, and F. Kampas, Annual Subcontract Report, 1 October, 1984 - 30 September 1985, Subcontract No ZB-3-03056-1 (SERI/STR-211-3406. Available NTIS: Order No. DE89000812).

18. A. E. Delahoy, T. Tonon, J. A. Cambridge, M. Johnson, L. Michalski, and F. J. Kampas, "Light Soaking Studies on Amorphous Silicon Photovoltaic Devices and Modules," Proc. 8th European Photovoltaic Solar Energy Conference (Kluwer, Dordrecht, 1988; I. Solomon, B. Equer, P. Helm, Eds) pp. 646-652.

19. D. Morel, Private conversation.

20. W. A. Nevin, H. Yamagishi, and Y. Tawada, Appl. Phys. Lett 54 (1989) 1226.

21. F. B. Ellis, Jr., and J. Houghton "Chemical Vapor Deposition of Silicon Dioxide Barrier Layers for Conductivity Enhancement of Tin Oxide Films" J. Mater. Res., Vo. 4, No. 4 (1989) pp. 863-872.

22. S. Kumar and G. Drevillon, J. Appl. Phys. 65 (1989) 863.

23. J. Morris, R.R. Arya, J.G. O'Dowd, and S. Wiedeman, "Absorption Enhancement in Hydrogenated Amorphous Silicon-Based Solar Cells" J. Appl. Phys. 67, 1079 (1990)

24. R.D. Wieting, M. Bölingen, J. Anderson and D.R. Willett, "Performance of Large Area Thin Film Si:H Modules: A Link Between Shunting and Stability" Conf. Record 21st. IEEE Photovoltaic Specialists Conference (IEEE, NY, 1990) pp. 1569 - 1573.

25. J. Macneil, A.E. Delahoy, F. Kampas, E. Eser, A. Varvar, and F. Ellis, Jr., "A 10 MW_p A-Si:H Module Processing Line" Ibid. pp. 1501 - 1505.

Document Control Page	1. SERI Report No. SERI/TP-214-4226	2. NTIS Accession No. DE91002167	3. Recipient's Accession No.

4. Title and Subtitle

Research on Stable, High-Efficiency, Large-Area, Amorphous-Silicon-Based Submodules

5. Publication Date
June 1991

6.

7. Author(s)
A.E. Delahoy, T. Tonon, J. Macneil

8. Performing Organization Rept. No.

9. Performing Organization Name and Address

Chronar Corporation
PO Box 177
Princeton, New Jersey 08542

10. Project/Task/Work Unit No.
PV141101

11. Contract (C) or Grant (G) No.

(C) ZB-7-06003-1

(G)

12. Sponsoring Organization Name and Address
Solar Energy Research Institute
1617 Cole Blvd.
Golden, CO 80401-3393

13. Type of Report & Period Covered
Technical report,
16 March 1989 - 15 October 1990

14.

15. Supplementary Notes
SERI technical monitor: W. Luft, (303) 231-1452

16. Abstract (Limit: 200 words)

This report describes research to develop same-band-gap, amorphous silicon, tandem-junction photovoltaic modules with areas of at least 900 cm^2. The goals are to achieve aperture-area efficiencies of 9% and modules that retain 95% of their original power output under standard light-soaking conditions. The approach involved depositing SiO_2/SnO_2:F onto soda lime glass via atmospheric-pressure chemical vapor deposition (APCVD) to provide a textured, transparent electrode; single-chamber radio-frequency (RF) glow discharge deposition of the hydrogenated amorphous silicon (a-Si:H) layers onto vertical substrates; sputter deposition of highly reflecting ZnO-based back contacts; and laser scribing of the a-Si:H and electrodes with real-time scribe tracking to minimize area loss. Studies of film uniformity were also performed, and performance data are presented for various single- and tandem-junction cells and modules.

17. Document Analysis
a. Descriptors
photovoltaics ; solar cells ; amorphous state ; silicon

b. Identifiers/Open-Ended Terms

c. UC Categories
271

18. Availability Statement
National Technical Information Service
U.S. Department of Commerce
5285 Port Royal Road
Springfield, VA 22161

19. No. of Pages
62

20. Price
A04

Form No. 0069E (6-30-87)